Nat. Hazards Earth Syst. Sci. Discuss., 1, 5935–6000, 2013
www.nat-hazards-earth-syst-sci-discuss.net/1/5935/2013/
doi:10.5194/nhessd-1-5935-2013

Natural Hazards and Earth System Sciences
Discussions
Open Access

Support to Aviation Control Service (SACS): an online service for near real-time satellite monitoring of volcanic plumes

H. Brenot[1], N. Theys[1], L. Clarisse[2], J. van Geffen[3], J. van Gent[1], M. Van Roozendael[1], R. van der A[3], D. Hurtmans[2], P.-F. Coheur[2], C. Clerbaux[2,4], P. Valks[5], P. Hedelt[5], F. Prata[6], O. Rasson[1], K. Sievers[7], and C. Zehner[8]

[1]Belgisch Instituut voor Ruimte-Aeronomie – Institut d'Aéronomie Spatiale de Belgique (BIRA-IASB), Brussels, Belgium
[2]Spectroscopie de l'Atmosphère, Service de Chimie Quantique et Photophysique, Université Libre de Bruxelles (ULB), Brussels, Belgium
[3]Koninklijk Nederlands Meteorologisch Instituut (KNMI), De Bilt, the Netherlands
[4]UPMC Univ. Paris 6; Université de Versailles St.-Quentin; CNRS/INSU, LATMOS-IPSL, Paris, France
[5]Institut für Methodik der Fernerkundung (IMF), Deutsches Zentrum für Luft und Raumfahrt (DLR), Oberpfaffenhofen, Germany
[6]Norsk Institutt for Luftforskning (NILU), Kjeller, Norway
[7]German ALPA, Frankfurt, Germany

[8]European Space Agency (ESA-ESRIN), Frascati, Italy

Received: 23 August 2013 – Accepted: 9 October 2013 – Published: 31 October 2013

Correspondence to: H. Brenot (brenot@oma.be)

Published by Copernicus Publications on behalf of the European Geosciences Union.

Abstract

Volcanic eruptions emit plumes of ash and gases in the atmosphere, potentially at very high altitudes. Ash rich plumes are hazardous for airplanes as ash is very abrasive and easily melts inside their engines. With more than 50 active volcanoes per year and the ever increasing number of commercial flights, the safety of airplanes is a real concern. Satellite measurements are ideal for monitoring global volcanic activity and, in combination with atmospheric dispersion models, to track and forecast volcanic plumes. Here we present the Support to Aviation Control Service (SACS, http://sacs.aeronomie.be), which is a free online service initiated by ESA for the near real-time (NRT) satellite monitoring of volcanic plumes of SO_2 and ash. It combines data from two UV-visible (OMI, GOME-2) and two infrared (AIRS, IASI) spectrometers. This new multi-sensor warning system of volcanic plumes, running since April 2012, is based on the detection of SO_2 and is optimised to avoid false alerts while at the same time limiting the number of notifications in case of large plumes. The system shows successful results with 95 % of our notifications corresponding to true volcanic activity.

1 Volcanic eruptions: a threat to aviation safety

Volcanic eruptions are known to emit large amounts of aerosols (silicate ash, sulphates and ice particles) and gases (mostly water vapour, CO_2, SO_2, H_2S and halogen species). The composition of each volcanic cloud is unique, as it is the result of a complex processes driven by the chemistry and motion of magma inside the mantle of the Earth and its ejection at the surface (Robock and Oppenheimer, 2003). Emission can sometimes have severe implications for the atmosphere, life on the Earth, and human society. Volcanic clouds can have a significant impact on atmospheric chemistry and climate, both locally and on a global scale (Robock, 2000; Oppenheimer et al., 2011), and can strongly affect human health in the vicinity of the volcano, but the effects of a volcanic cloud may even felt far from volcano (Forbes et al., 2003; Baxter et al.,

NHESSD

1, 5935–6000, 2013

1999). Volcanic ash and – to a lesser extent – sulphuric gases are also major hazards to aviation. The largest threat to aviation safety is that volcanic ash can damage plane engines and cause them to stall as a result of ash melting (Miller and Casadevall, 1999; Prata, 2009). Volcanic ash can abrade windscreens, damage avionic equipment and navigation systems, and reduce the visibility of the pilots. Moreover, sulphuric gases, such as H_2SO_4 and SO_2, may also damage the aircraft (paint and windows) and create sulphate deposits on and inside the engines. The gases might also be dangerous for the health of the passengers. In the past there have been several incidents as a result of encounters of aircraft with volcanic plumes (Casadevall, 1994; Casadevall et al., 1996; Guffanti et al., 2010). A significant difficulty in mitigating volcanic hazard to aviation is that, because of strong winds at high altitudes, fine ash can rapidly be transported over long distances (> 1000 km from the volcano) and in the process cross major air routes. As only a small number of the active volcanoes on Earth are regularly monitored using ground equipment, the use of space-based instruments (see Carn et al., 2008 and Thomas and Watson, 2010) is particularly relevant for aviation safety, as it enables the continuous and global monitoring of volcanic plumes in an effective, economical and risk-free way.

Nine worldwide Volcanic Ash Advisory Centres (VAACs) have been designated to advise civil aviation authorities in case of volcanic eruptions. These centres are part of the International Airways Volcano Watch (IAVW), established in 2002 by the International Civil Aviation Organization (ICAO) with the co-operation of numerous countries and several international organisations like the International Atomic Energy Agency (IAEA), the International Air Transport Association (IATA), the International Federation of Air Line Pilots' Associations (IFALPA), the International Union of Geodesy and Geophysics (IUGG) and the World Meteorological Organization (WMO). For more details see ICAO (2012). The nine VAACs each have their own area of responsibility, which together cover the whole globe. They make advisory information available en-route on the extent and movement of volcanic ash in the atmosphere. This information is then used by aviation safety control bodies and by pilots via SIGMET (SIGnificant

NHESSD
1, 5935–6000, 2013

METeorological Information) advisories. The VAACs provide volcanic ash forecasts using atmospheric dispersion models, by making use of all available information on volcanic clouds from observatories, pilot reports and measurements from the ground, aircrafts and above all from space instruments (mostly satellite imagery from geostationary instruments).

Until recently, a policy of zero tolerance regarding volcanic ash was applied by ICAO on airlines (Cantor, 1998). This regulation has changed with the introduction of ash concentration thresholds over Europe after the eruptions of the Icelandic volcanoes Eyjafjallajökull in April/May 2010 and Grímsvötn in May 2011, as both caused partial or total closure of airspace over many European countries and led to social and economic upheaval across Europe (IATA, 2010). The introduction of ash concentration thresholds translates to important needs and requirements for improved volcanic ash monitoring and forecasting services (see Zehner, 2010). These needs are:

– Early detection of volcanic emissions.

– NRT global monitoring of volcanic plumes, with open access and delivery of data.

– Quantitative retrievals of volcanic ash (concentration, altitude and particle size distribution) and SO_2 (concentration, altitude) from (but not limited to) satellite instruments. Ash data at high-temporal resolution from geostationary payloads (Prata and Prata, 2012) has priority.

– Accurate source term parameters: time-, particle size- and height-resolved ash source emissions for the entire eruptive period.

– Improved inversion techniques involving atmospheric models for forecasting ash dispersion and removal (Stohl et al., 2011).

– Validation of satellite observations.

In this paper, we give an overview of the Support to Aviation Control Service (SACS) which deals with the first two points listed above as it is an automated global system for the monitoring and warning of volcanic plumes. It makes use of NRT ash and SO_2 data products from satellite instruments operating in the UV-visible (OMI and GOME-2) and Thermal Infrared (IASI and AIRS) wavelength ranges. A system has been set-up to notify the users by e-mail in case of exceptional volcanic emissions. Here we present the strategy adopted to detect and monitor volcanic clouds. With examples of recent eruptions, we demonstrate the service and show the information available to the SACS user and detail the different aspects of our work.

2 Overview of SACS

The Support to Aviation Control Service is an ESA-funded project developed within the Data User Element (DUE-TEMIS, http://www.temis.nl) and the GMES Service Element (GSE-PROMOTE, http://www.gse-promote.org) programmes (Van Geffen et al., 2007). SACS is a collaborative project that currently involves the following partners: the Belgian Institute for Space Aeronomy (BIRA-IASB; leader), the Royal Netherlands Meteorological Institute (KNMI), the University of Brussels (ULB) and the German Aerospace Center (DLR). The SACS project is also indirectly supported by the following agencies/institutions: EUMETSAT (via the O3M SAF program), Centre National d'Etudes Spatiales (CNES), Finnish Meteorological Institute (FMI, Ilmatieteen Laitos), Norsk Institutt for Luftforskning (NILU), Jet Propulsion Laboratory (JPL), and the National Aeronautics and Space Administration (NASA). The primary objective of SACS is to support the VAACs (key users of the service) in their official tasks of informing aviation control organisations about the risks associated with volcanic activity. SACS is a free service available through a single user-friendly web portal (http://sacs.aeronomie.be) that centralises the data (near real-time and archive) in the form of maps (images) globally and for a set of pre-defined regions. This service is also linked to other European initiatives such as ESA SAVAA (http://savaa.nilu.no), VAST (http://vast.nilu.no) and EU FP7 EVOSS (http://www.evoss.eu), whose general aims

NHESSD
1, 5935–6000, 2013

H. Brenot et al.

are to define and demonstrate an optimal system for volcanic ash plume monitoring and prediction.

SACS delivers global data sets for sulphur dioxide (SO_2) and aerosol (ash) related to volcanic eruptions from measurements by space-based instruments. At the time of writing, SACS is based on polar sun-synchronous satellite instruments widely used to sound atmospheric composition and for meteorological and scientific applications: AIRS/Aqua (Aumann et al., 2000, 2003; Hofstadter et al., 2000), OMI/Aura (Levelt et al., 2006), GOME-2/MetOp-A (Munro et al., 2006) and IASI/MetOp-A (Clerbaux et al., 2009; Hilton et al., 2012). All SACS data retrievals are available in NRT (which means as soon as the data process allows to retrieve SO_2 and ash observations). Figure 1 shows the different sounders that SACS currently uses and their local overpass time. It shows the advantage of combining multiple sensors which have different overpass times in a single system as it allows the reliable and timely monitoring of volcanic plumes on the global scale. Note that until April 2012, the NRT SACS system also used data from SCIAMACHY/Envisat (Bovensmann et al., 1999) for which archive data can still be consulted. Table 1 presents a summary of the SACS products and their main characteristics: satellite platform, data type and availability, equatorial local overpass time, spatial resolution, retrieved quantity, data provider, units, delays of retrievals, swath widths, and global coverage. Note that the size of the footprint of each instrument (resolution in km^2) is an approximate value at nadir. A description of the different data products used in the SACS system is given in Sect. 3.

A notification system has been set-up to warn people (by email) in case of exceptional concentrations of SO_2, pointing them to a web page with relevant information on the location of the plume. Users also have the possibility to consult the notification service which compiles notifications of on-going or past eruptive events. Data archives contain the observations starting from September 2002 for AIRS, from January 2004 until April 2012 for SCIAMACHY, from September 2004 for OMI, from January 2007 for GOME-2, and from October 2007 for IASI.

NHESSD
1, 5935–6000, 2013

Title Page
Abstract | Introduction
Conclusions | References
Tables | Figures
◀◀ | ▶▶
◀ | ▶
Back | Close
Full Screen / Esc
Printer-friendly Version
Interactive Discussion

3 Description of satellite data products used by SACS

The detection of volcanic ash is far from trivial, especially for dispersed plumes. Most of the current satellite algorithms use differential absorption by ash between two channels, which can yield false detection in the presence of absorbing aerosols other than ash (e.g., desert dust). Conversely, satellite detection of SO_2 is more reliable and when it is present in the upper troposphere/lower stratosphere it is a more robust indicator of volcanic activity. Therefore, the SACS system at present only uses satellite SO_2 data products to trigger and issue plume notifications. SO_2 is often a good proxy for volcanic plumes and therefore possibly of volcanic ash (Thomas and Prata, 2011). This being said, not all eruptions are accompanied by detectable amount of SO_2 and even then it is not uncommon for ash and SO_2 to follow different trajectories because of differences in injection altitudes. For these reasons, SACS is providing both SO_2 and aerosol/ash information in NRT. In this section, we briefly present the different products from the five instruments listed in Table 1 and their main features.

3.1 SO_2 column retrievals from UV-visible sensors (SCIAMACHY, OMI, GOME-2)

The SCIAMACHY, GOME-2 and OMI instruments are UV-visible spectrometers measuring solar light backscattered by the atmosphere or reflected by the Earth (and hence can only measure during daytime). The observations are done in nadir viewing geometry, except for SCIAMACHY, which had alternating viewing modes in nadir and limb (not used here). Once a day, a direct measurement of the solar irradiance spectrum is also acquired. All three instruments have spectral channels covering the UV wavelength range (240–400 nm), where SO_2 has strong and distinctive absorption bands. The spectral resolution in the UV range is 0.2–0.6 nm.

The retrieved quantity from the three algorithms is the so-called SO_2 Vertical Column Density (VCD). It represents the SO_2 concentration integrated along the vertical axis and is generally expressed in Dobson Units ($1\,\mathrm{DU} = 2.69 \times 10^{16}$ molecules cm^{-2}). The SO_2 retrievals of SCIAMACHY (Van Geffen et al., 2007, 2008) and GOME-2 (Rix et al., 2009, 2012) use a Differential Optical Absorption Spectroscopy technique (DOAS, Platt and Stutz, 2008) where all measurements in a wavelength range from 315 to 326 nm are fitted to laboratory absorption data of SO_2 (and other atmospheric gases) to yield the SO_2 slant column, i.e. the SO_2 concentration integrated along the mean optical light path in the atmosphere. The OMI SO_2 retrieval is slightly different from SCIAMACHY and GOME-2 in that it uses only a small number of wavelengths (between 310 and 345 nm) in and outside the SO_2 band, following the Linear Fit algorithm (Yang et al., 2007) and it does not retrieve an SO_2 slant column as an intermediate step. Note that for all instruments, several background and offset corrections are generally applied, to ensure geophysical consistency of the data.

The SO_2 vertical column is obtained using radiative transfer calculations that account for important parameters influencing the UV light path in the atmosphere: solar zenith angle, viewing angles, clouds, atmospheric absorption and scattering, surface albedo. As the measurement sensitivity strongly depends on the altitude where SO_2 resides and because we have no knowledge what this altitude is prior to the measurement, the SO_2 vertical column estimation is provided on three hypothetical atmospheric layers representative of different scenarios of emissions: planetary boundary layer (typically the first km above the surface), upper troposphere ($\sim$ 6 km) and lower stratosphere ($\sim$ 15 km). The SO_2 images displayed in SACS all use the data assuming lower stratospheric plumes.

The SO_2 algorithms from OMI, SCIAMACHY and GOME-2 are able to detect similar SO_2 patterns for modest and strong eruptions. Figure 2 shows that the measurements (SO_2 VCD images from SCIAMACHY, GOME-2 and OMI for an eruption of Kilauea volcano in Hawaii, 17 May 2008) are able to consistently observe small (and low) SO_2 plumes. Despite the different overpass times, we can see a very good spatial correspondence of the location of the plume between the 3 instruments. To compare the SO_2 VCDs, a fixed latitude of 19.4° N has been chosen for the 3 instruments, and the measurements have been plotted as a function of longitude (Fig. 2d). A fairly good agreement between the VCD values is found, especially taken into account the fact

NHESSD
1, 5935–6000, 2013

the SO_2 plume is moving westward. This example shows and confirms that SO_2 VCD measurements from UV-visible instruments allow a good estimation and monitoring of volcanic emissions even for such a small eruption (the highest SO_2 VCD is 5.2 DU as recorded by GOME-2 during this day). Note that the operational cloud cover fraction products for all UV-visible instruments are also available on the SACS webpage as additional information. Note that the measurement times are indicated in UTC on all SACS images.

3.2 SO_2 index retrievals from thermal IR sensors (IASI and AIRS)

The IASI instrument is a Fourier transform spectrometer. The spectral coverage is from 645 to 2760 cm^{-1} (with no gaps) with a spectral resolution of 0.5 cm^{-1} (apodised) and a spectral sampling of 0.25 cm^{-1}. The AIRS instrument is an echelle grating spectrometer covering the range between 650 and 2665 cm^{-1} (with gaps) and a spectral resolution of 0.5–2 cm^{-1}. The instruments are operating in a nadir view with typical footprints (circular to elliptical depending on the position on the swath) of 12 and 15 km diameters (at nadir), for IASI and AIRS respectively. Both sensors measure the spectrum of the outgoing thermal radiation emitted by the Earth-atmosphere system (and hence can operate during both day and night).

Both IR instruments cover the strong ν_3 (asymmetric stretch) SO_2 absorption band around 1362 cm^{-1}. For AIRS, three wavenumbers are used (1395 cm^{-1}, 1327 cm^{-1} and 1328 cm^{-1}), while the IASI algorithm is based on measurements around 1408 cm^{-1}, 1372 cm^{-1} and 1385 cm^{-1}. The AIRS L1 data are provided in near real-time by NASA's Earth Observing System Data and Information System (EOSDIS, https://urs.eosdis.nasa.gov), and the SO_2 retrievals are processed by BIRA-IASB using the algorithm from NILU. The retrieval scheme of AIRS is a two-step process with a first step to identify pixels that contain SO_2, and a second step to adjust the amount of SO_2 based on off-line radiative transfer calculations (see details in Prata and Bernardo, 2007). The retrievals from IASI SO_2 are provided in NRT by the ULB (http://cpm-ws4.ulb.ac.be/Alerts). The IASI SO_2 algorithm (see details in Clarisse et al., 2012) also involves the conversion of the measured signal into an SO_2 vertical column by making use of a large look-up-table and EUMETSAT operational pressure, temperature and humidity profiles. These are only available for data with L2 information. To ensure a maximum amount of IASI data, only the brightness temperature difference index is used in the NRT treatment of SACS.

Figure 3 shows IASI and AIRS SO_2 images from SACS after the beginning of the eruption of Nabro's volcano (Eritrea). IASI was the first instrument to observe the SO_2 plume at 06:25 a.m. and 08:05 a.m. UTC (for two consecutive orbits) on 13 June 2011. Nevertheless these observations did not cover the full plume. At 10:50 a.m., a full coverage of the plume was possible by combining IASI with AIRS measurements. This illustrates the benefit of our multi-sensor approach. As a side note, the delay time for receiving the data was about 1 h50 and 1 h30 for IASI and AIRS, respectively.

3.3 Absorbing aerosol index retrievals from UV-visible sensors (SCIAMACHY, OMI, GOME-2)

The Absorbing Aerosol Index (AAI) indicates the presence of elevated absorbing aerosols in the atmosphere. It is often named the residue, the spectral contrast anomaly, or simply aerosol index. Because the presence of ash can be the dominant part of the AAI detection, SACS provides these products in near real-time. The AAI separates the spectral contrast at two ultraviolet wavelengths caused by absorbing aerosols from that of other effects, including molecular Rayleigh scattering, surface reflection, gaseous absorption, and aerosol/cloud scattering (Herman et al., 1997; Torres et al., 1998).

The UV wavelengths used are 340 nm and 380 nm for SCIAMACHY and GOME-2, and 354 nm and 388 nm for OMI. Note that AAI retrieval is possible over cloud covered areas and is performed equally well over ocean and land (except over ice). However, the final AAI products are sensitive to calibration issues and sunglint over the ocean and therefore ad-hoc flags are applied. Figure 4c and d show an example of AAI images from the UV-visible sensors GOME-2 and OMI. Ash emitted during the Grímsvötn eruption is clearly identified.

3.4 Ash index retrieval from the thermal IR sensors (IASI, AIRS)

Clarisse et al. (2010, 2013) have demonstrated the potential of hyperspectral thermal infrared sounders to detect volcanic ash with a high sensitivity and differentiate it from other airborne aerosol (including windblown sand). The IASI and AIRS ash index products used in SACS are based on a three-step process (see Clarisse et al., 2013 for details). The first step calculates the relative distance (weighted projection) between the measured spectra and fixed ash spectral signatures. Based on the magnitude of these distances, only those observations are kept which are likely to be ash (called ash candidates). The second step finds the subset of observations which are almost certainly ash by imposing very strict criteria based on absolute distance criteria (called high confidence detections). The third steps considers spatial context to promote ash candidates to low and medium confidence detections in the neighbourhood of high confidence detections. The procedure ensures a very low false detection rate (because of step 2), while at the same time identifying as much as possible ash in the neighbourhood of high confidence detections (because of steps 1 and 3). Figure 4a presents the AIRS detection of ash at 03:40 UTC on 22 May 2011. Note that IASI was the first instrument on a polar orbiting satellite able to clearly distinguish ash emitted at the start of the Grímsvötn eruption at 20:45 UTC on 21 May 2011. Figure 4b shows the IASI ash detection at 10:30 UTC on 22 May. We can see in Fig. 4c and d the displacement of the ash cloud during the next 2 days (ash detected by AAI retrievals from GOME-2 and OMI).

NHESSD
1, 5935–6000, 2013

3.5 Limitations of satellite products in detecting volcanic plumes

3.5.1 SO_2 products

Because of competing water vapour absorption in the same IR wavelength window as SO_2, the vertical sensitivity of IASI and AIRS to SO_2 is limited to the atmospheric layers above 3–5 km depending on the humidity vertical profile. This limitation might seem serious, but in the context of aviation it is actually an advantage as the detection of SO_2 by these two sensors means that SO_2 is present at altitudes where airplanes spend most of their travel time. This fact combined with four overpasses per day make the IR sensors a central component of the SACS system. As a complement, the UV sensors are characterised by a relatively good measurement sensitivity for SO_2 down to the surface. While this allows monitoring of low altitude volcanic degassing, it also renders the measurements sensitive to anthropogenic emissions. As most of the SO_2 pollution hotspots are confined to a limited number of regions (China, South Africa, Siberia), the SACS system can easily be tuned to avoid false notifications there. As a general comment, SO_2 retrievals are also affected by clouds and instrumental noise (especially at high solar zenith angles for the UV sensors). The latter generally shows up in the SO_2 images and evolves as the instrument is degrading over time.

3.5.2 Aerosol products

Besides the fact that the aerosol products are qualitative products (indexes), measurements from UV-visible sensors are sensitive to all types of absorbing aerosols (desert dust, biomass burning aerosols, volcanic ash) and are therefore not purely selective for ash. However, the combined detection of both elevated aerosol and SO_2 is highly selective for the volcanic plume (in fact even more than SO_2 detection alone). Note that the ash product of IASI and AIRS sensors yields very few false detections. But it should be noted that because of the strict conditions of step 2, low concentration ash plumes are often not detected in the current implementation.

NHESSD
1, 5935–6000, 2013

3.5.3 Known anomalies impacting the data

The Earth's dipolar magnetic field is offset by about 500 km from the rotational axis. As a result of this, the inner Van Allen belt (doughnut-shaped regions of high-energy charged particles) is on one side closer to the Earth's surface than the other side. This region is named the South Atlantic Anomaly (SAA) and it covers a part of South America and the Southern Atlantic Ocean: it lies roughly between latitudes 5 and 40° S, and between longitudes 0 and 80° W (the precise strength, shape and size of the SAA varies with the seasons). This dip in the Earth's magnetic field allows charged particles and cosmic rays to penetrate lower into the ionosphere (at ~ 500 km of altitude). Low-orbiting satellites, such as Envisat, Aura and MetOp-A, pass daily through the inner radiation belt in the SAA-region. Upon passing the inner belt, charged particles may impact on the detector, causing higher-than-normal radiance values, which in turn decreases the quality of the measurements, notably in the UV. The SAA affects the SO_2 retrievals and results in noise artefacts, as is visible in Fig. 5a and b. Thanks to its design which gives it better protection to radiation than other sensors, OMI is less affected by the SAA than SCIAMACHY or GOME-2 (as can be seen Fig. 5c).

The OMI instrument has started to suffer from a so-called "row anomaly" since 25 June 2007. This anomaly affects particular viewing direction angles, corresponding to rows on the CCD detector. The row anomaly has increased over time (see www.knmi.nl/omi/research/product). Currently, the affected rows are not treated in SACS, leading to a reduction in the data coverage. Several off-line schemes to correct for the row anomaly exist (e.g. Yan et al., 2012) but are not implemented yet in the NRT data-processing.

4 Global monitoring of volcanic SO_2 and ash emissions

In this section we present results from the SACS global monitoring system of SO_2 emissions and the strategy adopted to warn users of exceptional SO_2 concentrations.

NHESSD
1, 5935–6000, 2013

4.1 Temporal and spatial sampling

It is important to know precisely the time and space sampling of the SACS monitoring system. Because of the use of polar-orbiting satellites with different overpass times, some geographical regions are observed more frequently than others. To evaluate the revisiting frequency of SACS, we have defined seven geographical latitude zones (see Fig. 6a) and we have estimated, based on data of October 2012, the percentage of the areas that have been observed at least once by one of the satellite instruments (OMI, GOME-2, IASI, AIRS). The calculation was done for several time intervals (see e.g. the coverage of the Earth by SACS after 8 h of monitoring in Fig. 6b). Table 2 presents the results for the different zones and time durations. A set of two parameters has been evaluated: pxl is the percentage of the region of interest sampled by the SACS system; and max is the maximum number of overpasses. From Table 2, it can be seen that with four instruments, SACS monitors in near real-time any location in the world within a 24 h interval. The percentage value drops to 99.5 %, 95 %, 90 %, 75 %, 60 %, 50 % and 30 % for periods respectively of 12, 8, 6, 4, 3, 2 and 1 h.

Also apparent is the higher sampling rates for high-latitude regions due to overlapping orbits. This is particularly interesting for Icelandic volcanoes (zone E) that will be sampled e.g. every 2 h 50 % of the time (see Table 2). Note that the geographical coverage of D-E-F zones depends on the day of year. For example in December, the coverage of Iceland is less good (due to the SZA limit for UV-vis instruments). Nevertheless, because the IR sensors are not affected by the SZA limit criteria (day and night measurements), the coverage of the high-latitude regions always takes advantage of overlapping orbits over North and South Poles.

4.2 SACS strategy for volcanic SO_2 notifications

Here, we detail the implementation of the global multi-sensor notification system for SO_2. It requires two steps: (1) proper establishment of warnings criteria for the different sensors, (2) combining the information from the sensors in one system.

Particular attention is given to the avoidance of false notifications (due to noise or retrieval failures) or overly frequent/redundant notifications (caused by highly dispersed plumes).

4.2.1 Criteria for SO_2 notification

The criteria for detection of exceptional SO_2 concentrations from the five instruments has been derived from the analysis of historical results (see Table 1 for the data periods considered). Each instrument and retrieval method has different characteristics, therefore for each data source different notification threshold values have been established. Note that, even though it no more provides data, SCIAMACHY is included here because it has been used in the past and notifications based on its data are in the SACS archive.

SO_2 notification from UV-visible sensors

The instrumental noise on the UV-visible data is a limitation and can lead to false notifications. For this reason, a first selection criterion is based on the maximum observed value for the SO_2 column which must exceed the relevant threshold. An additional criterion is based on the neighbouring pixels (inside a threshold radius, see Table 3 and Fig. 7), for which the observed SO_2 column for more than half of the observations must also exceed the threshold value. A notification is generated only when both criteria are fulfilled. An illustration is given in Fig. 7 for GOME-2 for an SO_2 plume from the Copahue volcano (23 December 2012).

Another limitation of UV-visible sensors comes from the South Atlantic Anomaly (see Sect. 3.5.3). To avoid false notifications in this region, a more strict threshold value is considered (see Table 3). Note also that special settings are used for SO_2 plumes from small eruptions and degassing, in that the system considers lower threshold values for measurements close to a given volcano (distances less than 300 km). Finally, one more limitation of UV-visible sensors is that they are sensitive to anthropogenic SO_2

NHESSD
1, 5935–6000, 2013

emissions. To avoid false notifications, more strict criteria are used for some specific areas (West China, Central North Russia and South Africa).

SO_2 notification from thermal IR sensors

IASI and AIRS are much less or not at all affected by instrumental noise, the SAA, or pollution. For IASI, rather than considering threshold values based on VCD, the criteria apply directly on the measured Difference of Brightness Temperatures (called DBT and expressed in Kelvin [K]), and is therefore straightforward. The threshold values (DBT and VCD) used are given in Table 3 for respectively IASI and AIRS, and they produce almost no false notifications.

4.2.2 SACS multi-sensor warning system

The SO_2 warning service relies on pre-defined geographical regions. SACS sends a notification to users as soon as a new volcanic plume is detected. If within a period of 12 h, a plume is detected again in the same region no new notification is generated (to avoid sending redundant information). An illustration of the SACS multi-sensors warning system is presented in Fig. 8. The different parts are described in more detail below.

SO_2 notification for a dedicated region

As soon as SACS harvests new SO_2 observations (from one of the instruments), the first step is the analysis of the data using the criteria defined in Sect. 4.2.1. After a volcanic eruption, there are potentially multiple warnings generated by the system. For this reason, it has been decided to consider a set of world regions of 30° by 30° plus two polar regions polewards of 75° in latitude. Figure 9 shows the locations (and associated name/number) of the 62 regions of the SACS system. Note that the same regions are used in the near real-time monitoring and archive services to display the

SO_2 and ash images. As soon as a notification is issued, the related region is flagged "ON".

Check of the warning status

The second step is to check the "warning status" of this region. If there is no on-going notification for this region (meaning no notification since 12 h), the warning status can possibly become ON. The system compares the time of observations with the processing time. If the delay is less than 8 h, the notification is issued. This set-up enables to provide timely information to the users and also to avoid issuing too many notifications (maximum one notification per region and per 12 h).

E-mail notification

Important information related to the warning is gathered into a notification sent by email to users who subscribed to SACS (http://sacs.aeronomie.be/alert/subscribe.php). The email notification (see also the example shown in Fig. 10) contains: the time of the notification and the instrument, the region number, some details about the processing, a link to a dedicated web page generated by the system, coordinates of the maximum SO_2 signal along with the date and time of observations (UTC), a flag indicating whether a cloud correction has been applied or not, and finally the solar zenith angle.

Note that a solar zenith angle cut-off is used for each UV-visible sensor depending on the day of the year. The values have been determined empirically to have the best coverage while limiting the increase in the noise (instrument-specific).

Dedicated SO_2 notification's web page

An example of a web page generated by SACS using GOME-2 data for a specific notification is shown in Fig. 11. This notification was sent to the users 1 h01 after MetOp-A passed over this area. The page shows a box with the information of the email notification (time of measurement, location of the warning, SZA, maximum SO_2 value, and the use of cloud data in calculations), and the images of SO_2 and aerosols/ash side-by-side. Below the SO_2 image, one can find two links to the same image but using different mapping tools (interpolated image using the Generic Mapping Tools from the University from Hawaii, see http://gmt.soest.hawaii.edu, and a Google-Earth file, see http://www.google.com/earth). For the UV-visible instruments, there is also a link to the corresponding cloud cover fraction (CCF) image. In case of a IASI notification, in addition to the SO_2 brightness temperature index image there is also a link to the SO_2 VCD image. As a complement, a map showing the volcanoes in the region (with a link to a listing including more information about each of them) is also provided on this web page. Furthermore, a direct link to the near real-time monitoring web page is given with all corresponding SACS images (for all instruments), and a link to the data (files or link to data providers), for the region considered.

Confirmation of SO_2 notification

For the example shown in Fig. 11, IASI also detected SO_2 signal and ash in the region 112 (see Fig. 12) and acted as a confirmation. In fact the processing of IASI was just 3 min after the one of GOME-2, which took place at 23:42 UTC, as show Fig. 10. No notification has been sent to the users, as there already was a notification based on GOME-2, but the dedicated web page has been automatically updated with the notification box for the IASI warning using the same displaying template. Note that two and ten hours after this notification from GOME-2, two others confirmations from AIRS and IASI took place.

Update of SO_2 warning archive

As soon as a warning is detected by the system, the warning archives are automatically updated on the SACS web site. The warning subpage allows the users to select the instruments of interest, for a given month/year and to visualise a map with the location of all the corresponding warnings (see next section). For a given region, a minimum

Discussion Paper | Discussion Paper | Discussion Paper | Discussion Paper |

NHESSD

1, 5935–6000, 2013

An online service for near real-time satellite monitoring of volcanic plumes

H. Brenot et al.

delay of 12 h separates the time between two warnings, as explained above. The map of the warnings is an interactive map. When moving the cursor on a warning point, the user can visualise the images corresponding to the warning. In addition to this interactive tool, a common list with all the warnings (chronologically sorted) is also available with the relevant links to the different webpages.

4.3 Nine years of data and notifications archive

Although the multi-sensor notification system is only operational since April 2012, nine years of historical data have been reanalysed for the development of the warning service. This section presents an overview of all the notifications identified by SACS using the five sensors. For each year (from 2004 to 2012), an image of all the notifications is shown with a highlight of the main events. This tool, available on the SACS portal, allows any interested person to investigate historical eruptive emissions in a quick and user-friendly way. Note that our system also allows the monitoring of small volcanic eruptions which might not always lead to a notification.

4.3.1 Notifications from 2004 to 2006 (SCIAMACHY, OMI, and AIRS)

Data from the SCIAMACHY, OMI, and AIRS instruments are available for this period. The main volcanic activity detected by SACS in 2004 is in the Independent State of Papua New Guinea, the archipelago of the Republic of Vanuatu, and the Democratic Republic of Congo (DRC), as shown in Fig. 13a. The borderland between Rwanda, the DRC and Uganda is one of the most active regions containing eight volcanoes, including Mount Nyamuragira and Mount Nyiragongo which were both erupting on 25 May 2004. Details about the satellite monitoring of SO_2 emissions from Nyiamuragira from 1979 to 2005 can be found in Bluth and Carn (2008). Figure 13a presents also several SO_2 notifications over Europe in 2004. During the first week of November, an eruption occurred in Iceland (Grìmsvötn volcano). Volcanic ash from the eruption fell as far away as mainland Europe and caused short-term disruption of

NHESSD
1, 5935–6000, 2013

airline traffic into Iceland. Assuming an ash density of 2200 kg m^{-3} and using dispersion models from the VAACs, Witham et al. (2007) gives an emission up to 9.50×10^{12} g h^{-1} for the larger plume, that corresponds to an erupted mass of 3.3×10^{11} kg and a volume of 0.15 km^3 over the 35 h release period. Note that at this time of the year, the thermal IR sensor (AIRS) was the best instrument (best coverage and time laps between observations) to monitor the volcanic plume.

The volcanic activity in DRC (Galle et al., 2005) and in Galapagos and Vanuatu has continued in 2005 as can be seen in Fig. 13b. The signatures of two additional eruptions are also visible: (1) the submarine eruption of the Japanese Fukutoku-Okanoba volcano, located 6 km northeast of the pyramidal island of Minami-Iwojima (about 1300 km south-west of Tokyo); (2) the eruption of the Sierra Negra volcano, Galápagos, Ecuador. After 26 yr being inactive and six months after an earthquake on an active fault, the volcanic activity of the Sierra Negra raised again on 22 October 2005 with a fissure opening inside the rim of the caldera. This eruption emitted a volcanic cloud with an estimated volume of 150 millions m^3 of gas with a 2 km long curtain of lava fountains (Geist et al., 2008). During this effusive eruption, a huge amount of gas and particles was ejected in the low troposphere. The plume of SO_2 and ash reached an altitude estimated below 5 km (Yang et al., 2009). At the end of October 2005, atmospheric emissions of this volcano ceased.

In 2006, volcanic activity has been detected by SACS (Fig. 13c) in the Andes Cordillera (Colombia and Peru), but the three strongest eruptions occurred in other parts of the world: (1) on 6 October, a large explosive eruption took place at Rabaul volcano (Papua New Guinea), sending a plume of gas and ash up to the lower stratosphere. Several notifications have been issued by SACS showing the volcanic cloud traveling westward; (2) the Nyamuragira volcano was also active in 2006. A strong eruption began in the night of the 27 November (see e.g. Prata and Bernardo, 2007). The volcanic cloud initially moved north-eastward to finally travel to the west and pass over Pakistan and India; (3) the 20 May eruption of Soufrière Hills (Montserrat, British Overseas Territory) released a volcanic cloud which travelled over a very long

NHESSD
1, 5935–6000, 2013

distance (more than 18 000 km westward). A large dome collapse was accompanied by a large explosion, producing an ash column of about 18 km height (Prata et al., 2007). The movement of this volcanic cloud has been monitored during 23 days (see Fig. 14), drifting westward and causing diversion of many planes. The 20 May, at 17:02 UTC, the OMI sensor measured a VCD up to 122.2 DU. Several days after the eruption, the wind rapidly dispersed the volcanic cloud on the north-east and the south-west directions (22 and 24 May, Fig. 14). Note that for this date, the OMI sensor was not yet affected by the row anomaly and was still able to provide global coverage.

4.3.2 Notifications from 2007 to 2012 (SCIAMACHY, OMI, AIRS, GOME-2 and IASI)

Since 2007, SO_2 observations from the GOME-2 and IASI instruments became available and have been included in SACS. Volcanic emissions in 2007 have been observed by our system for some volcanoes of the Russian Federation (located in the Northern Kurile Islands and in Kamchatka), as shown in Fig. 15a. In January 2007, the Kliuchevskoi volcano started another eruption cycle. On 28 June, this volcano began to experience the largest explosions so far recorded in that eruption cycle, disrupting air traffic from the United States to Asia and causing ash falls on Alaska's Unimak Island. Volcanic activity has also be monitored by SACS in many other regions on Earth (although not all events are relevant for aviation), notably in Papua New Guinea (Rabaul volcano), the archipelago of Vanuatu (Ambrym and Lopevi volcanoes), in Ecuador (Tungurahua volcano), the Bonin Islands of Japan (Fukutoku-Okanoba), Italy (Etna), and in Ethiopia (Manda Hararo). The two largest eruptions of 2007 were observed at Jebel al-Tair Island (Yemen) and at Réunion Island (France).

The Jebel al-Tair eruption started unexpectedly on 30 September 2007 after 124 yr of dormancy. SO_2 emitted during the initial eruption travelled rapidly northward over Egypt and eastward over Pakistan and India (Clarisse et al., 2008). The volcanic plume reached the low stratosphere at an altitude of about 16 km (Eckhardt et al., 2008; Clarisse et al., 2008; Yang et al., 2009). The eruption of Piton de la Fournaise

(Réunion Island) started during the night of 30 March 2007. This was the largest eruption in 100 yr in this region (Deroussi et al., 2009). On 2 April, the opening of a fissure produced a lava flow that reached the sea with a flux estimated at $100\,m^3\,s^{-1}$. A degassing up to $1800\,kg\,s^{-1}$ was estimated for this day by Tulet and Villeneuve (2011). Their study of the temporal evolution of the SO_2 emission shows a budget of 230 kt. This eruption stopped on 1 May.

The SACS notifications of 2008 are presented in Fig. 15b. Besides a few eruptions on the Galapagos islands (Cerro Azul volcano) and the eruption of Dalafilla volcano (Ethiopia), the two most significant explosive eruptions happened at the Okmok and Kasatochi volcanoes (Aleutian Islands, Alaska, USA), respectively, in July and August. These two eruptions have been studied extensively and more information can be found in the literature (e.g. Prata et al., 2010; Karagulian et al., 2010; Krotkov et al., 2010; Clarisse et al., 2011). These strong eruptions caused a real threat to air traffic over the North American continent (see affected regions Fig. 15b).

Figure 16 presents the SO_2 cloud from Kasatochi as observed by IASI on 10 and 11 August (interpolation with a grid of 0.25° by 0.25°). The ash images from IASI (showing the level of confidence of the detection) have been superimposed over the SO_2 images. The ash and SO_2 clouds show a similar pattern on 10 August (see Fig. 16a). Note that ash observed with a low level of confidence over the south of Alaska and the west of Canada is an artefact in the analysis of the spectrum and the process of ash detection. The volcanic plume emitted by Kasatoshi was a SO_2-rich cloud (up to 676.4 DU on 8 August). We can see on 11 August that the detected ash cloud is smaller than the SO_2 cloud (see Fig. 16b).

Two months after Kasatochi eruption, Dalaffilla volcano erupted on 3 November. This volcano, located in the Afar region of Ethiopia, is one of the six volcanoes in the Erta Ale Range. We can see in Fig. 15b that a few days after this eruption, which was the largest observed in Ethiopia in historical times, the volcanic cloud generated six SO_2 notifications over India and the south of China.

NHESSD
1, 5935–6000, 2013

Three major eruptions that occurred in 2009 were identified by the SACS warning service (Fig. 15c): redoubt volcano in Alaska, Fernandina volcano in Galápagos islands, and Sarychev volcano in the Kuril islands. The explosive eruption of Sarychev (11–19 June 2009) emitted a huge amount of ash and SO_2 into the atmosphere for a range of altitudes of 10–16 km (Carn and Lopez, 2011; Clarisse et al., 2012). The mass of the SO_2 plume was estimated to be 1.2 ± 0.2 Tg by Haywood et al. (2010). This eruption, which was one of the 10 largest stratospheric injections in the last 50 yr, significantly affected the radiative budget of the atmosphere (Haywood et al., 2010). Images of the SO_2 and ash clouds observed by AIRS are shown in Fig. 17 (ash image superimposed over the SO_2 image). We can see that the ash detection (with a low level of confidence) over the Russian land on the north of the Sea of Okhotsk is an artefact. On the morning (UTC time) of 16 June, SO_2 and ash cloud are well co-located (see Fig. 17a). Note that the first SO_2 plume was emitted two days before and was observed on the West coast of USA. Figure 17b shows the SO_2 cloud observed on the afternoon of 17 June. The ash cloud detected by AIRS is located over the Sakhalin Russian Island. No ash was detected by AIRS over the Pacific ocean.

Figure 18a shows all the SO_2 notifications identified by SACS for the year 2010. Many regions were affected by volcanic activity. The 2010 eruptions of Eyjafjallajökull volcano in Iceland were relatively small, but unusual meteorological conditions brought volcanic ash clouds over Europe, causing enormous disruption to air traffic across western and northern Europe over an initial period of six days in April 2010 (Zehner, 2010). Additional localised disruption continued into May 2010. The eruption was declared officially over in October 2010, when snow falling on the glacier did not melt anymore. From 14 to 20 April, ash covered large areas of northern Europe when the volcano erupted (see Fig. 19 with images of the level of confidence of ash detection from AIRS and IASI from 14 to 17 April). Most of the airports of Northern Europe were closed by the authorities. During these days, the quantity of SO_2 observed by UV-visible and IR satellites was low (less than 5 DU), possibly due to local chemical reactions between SO_2 and water vapour creating sulfides or sulphuric acid. In May 2010, during

NHESSD
1, 5935–6000, 2013

the second phase of emissions, a more significant amount of SO_2 was measured (up to 28.6 DU for AIRS, on 6 May).

The strongest eruption of 2010 was the one of Merapi on 3 November on the Island of Java, Indonesia. Rapid ascent of magma from the depths of the volcano and the collapse of the lava dome put the large population living around the volcano in danger. People had to move away from their homes around the flanks of Merapi. For the first time, remote sensing (ground deformation by aperture radar, and monitoring of gas emissions by spectroscopic technique), together with the monitoring of the seismicity and the ground deformation by geodetic technique, provided precursory signals of this volcanic crisis, avoiding the death of several thousand people living around (Surono et al., 2012). Explosive and effusive phases took place and released a mass of SO_2 of about 0.44 Tg. The altitude of the SO_2- and ash-rich plume was estimated to be about 12 km. Figure 20 presents SO_2 and ash measured by IASI on 5 November. Ash and SO_2 were monitored respectively by IASI during 10 and 15 days after the start of the eruption. The five instruments used by SACS (with their space- and time-complementarities) identified many SO_2 notifications (see Fig. 18a) and allowed a good monitoring of the Merapi's eruption and its volcanic cloud (eastward movement and then southward).

The largest number of notifications of the SACS system to date occurred during the year 2011 (Fig. 18b). The three major events of 2011 were the eruptions of the Icelandic Grìmsvötn volcano (21–28 May), the eruption of the Chilean Puyehue-Cordón Caulle volcano (4–7 June), and the eruption of the Eritrean Nabro volcano (12 June–7 July). A characteristic feature of the Grìmsvötn eruption is that a large amount of SO_2 was ejected northwards while the ash cloud went to the southeast (see GOME-2 image Fig. 21). In this figure, the image of the absorbing aerosols index has been superimposed onto the SO_2 image. A null, low, medium and high level of aerosols/ash detected by GOME-2 corresponds respectively to AAI under 2, AAI of 2.5, AAI of 3, and AAI over 3.5. Aerosol detection on the north coast of Norway is not related to the Grìmsvötn eruption. The SO_2 cloud, which travelled over Canada and came back over

Europe, was monitored during 3 weeks. The ash cloud, which travelled over Europe, was under the limit of detection 3 days after the start of the eruption.

On 4 June 2011, the eruption of the Puyehue-Cordón Caulle volcano started. Out of the nine years the SO_2 notification archives span, this eruption is the most ash-rich recorded by our system. The volcanic cloud emitted was an ash-laden plume. During the first two days of this eruption, the SO_2 and ash clouds were collocated. Afterwards, the volcanic cloud dispersed and circled around the South pole (see Fig. 22). Within a few day, the cloud of ash covered the main part of Southern high latitudes. Note that for this particular eruption, that occurred during the Austral winter, the UV sensors had limited coverage and IASI and AIRS were the only sensors able to track globally the volcanic plume. The SO_2 and ash clouds were observed by IR sensors respectively during 3 and 5 weeks. The volcanic ash emitted by Puyehue consequently disturbed the air traffic of the Southern Hemisphere during the month of June 2011 in Chili, Argentina, Uruguay, Brazil, South Africa, Australia and New Zealand.

During the night of 12 June 2011, the Eritrean Nabro volcano started to erupt (see Fig. 3). This explosive eruption ejected a huge amount of SO_2 in the atmosphere, threating international routes from the Far East to Europe. On 14 June, the Nabro volcano spewed a volcanic plume across the route of many flights over East Africa and the Middle East. Satellite information was critical in monitoring the journey of the volcanic cloud. We can see in Fig. 3 the cloud of SO_2 detected by IASI and AIRS on 13 and 14 June. Figure 23 shows the SO_2 plume observed by IASI during the night of 15–16 June. The amount of ash emitted by Nabro for this eruption was very low (and largely undetected by IASI and AIRS), while the ash emitted by the Puyehue volcano was still detected by IASI in Fig. 23.

Figure 18c shows the SACS notifications for 2012. Continuous activity was recorded at the Nyamuragira volcano (DRC). Summit eruptions of Etna (Italy) were also detected by SACS in January–April 2012, and again in July–October 2012, but no strong disruption of air traffic occurred. On 1 September 2012, an explosive eruption took place at Bezymianni volcano (Kamchatka), producing an SO_2 and ash cloud (see

Figs. 11 and 12). With a cloud rising to an altitude of about 10 km, the Tokyo VAAC sent out an ash-cloud aviation warning and the major intercontinental routes that pass in that area were cancelled. Less than two months after this eruption, a nearby volcano, the Tolbachik, erupted on 27 November. The main part of the volcanic ejection drifted north and northwest (NNW), as observed by IASI and AIRS sensors. At this time of the year and for this location, the thermal IR instruments were the only instruments used by SACS that were able to monitor the volcanic cloud. The ash advisory board from the Tokyo VAAC reported of an ash cloud at an altitude of 10 km, spreading to the NNW. Despite this, no ash was detected by the instruments used by SACS.

The last 2012 eruption which caused a disruption to air traffic, was the eruption of the Chilean Copahue volcano (23–25 December). An SO_2-rich plume associated with ash emissions was spewed into the sky (Fig. 24). The volcanic plume was transported over Chile and aviation authorities in South America warned airlines to avoid the area. Contrarily to the previous eruption of Puyehue in June 2011, the Copahue's volcanic cloud was not particularly ash-rich. We can see in Fig. 24 that for the first day of this eruption, SO_2 and ash clouds took the same trajectory, nevertheless the high concentrations of SO_2 and ash are not exactly at the same locations.

In this section, we have shown the major volcanic events which have disturbed air traffic during the last 10 yr. We can see the uniqueness of each eruption. This diversity is characterised by different volcanic cloud compositions (sometimes SO_2-rich and/or sometimes ash-rich) driven by to specific meteorological conditions occasionally dispersing the plume over several continents. To synthetize the full performance of our notification system from 2010 to 2012, the diagnosis of SACS monitoring of the volcanic activity is presented in the Appendix A.

5 Conclusions and perspectives

Ash emitted from volcanoes poses a significant threat to aircraft because once it is sucked into the aircraft's engines, it readily melts and can potentially cause engine

NHESSD
1, 5935–6000, 2013

failure. Europe, North America, the north Atlantic and Asia regions have the highest air traffic densities with an estimated rate of growth of about 2–5 % per year during the period 1990–2050 (ESCAP, 2005). With the increase of commercial and freight air traffic, the increase of volcano surveillance is a critical need for future aircraft safety (Prata, 2009).

The near real-time monitoring of ash and SO_2 from satellite sensors is essential for the international Volcanic Ash Advisory Centres (VAACs). Focussing on instruments onboard polar orbiting platforms, this study presents the Support to Aviation Control Service (SACS). This free service provides images of SO_2 and ash in near real-time on a global scale via a web interface (http://sacs.aeronomie.be). We created a notification system and demonstrated that it is able to detect all volcanic events that occurred during the last decade that were a threat to aviation. The current system uses in synergy data products from UV-visible sensors (OMI and GOME-2) and thermal IR sensors (AIRS and IASI) with a revisiting time of (at least) 6 h anywhere on Earth. We have assessed the limitations of our system and estimated the success rate of the notifications. At the time of writing, the SACS multi-sensor warning system generated 444 notifications (emails sent with information and links to images) since its activation in April 2012. With a number of 17 false notifications provided by UV-visible sensors (mainly due to observations at high solar zenith angle or during an eclipse of the sun), more than 95 % of the notifications have been successful. The warning system actually considers only the SO_2 detection and not the more difficult detection of ash, however for each SO_2 notification and dedicated webpage creation, an associated image of ash/aerosols is provided. In particular, a level of confidence is included for the observations of ash from IASI and AIRS (Clarisse et al., 2013).

Finally, the next objectives for our service are:

- to incorporate more sensors in the system (in particular IASI and GOME-2 on MetOp-B), and possibly also improved satellite data products for ash (as an outcome of the on-going SACS2 project);

NHESSD
1, 5935–6000, 2013

– to operate a new notification system selective for the detection of ash using thermal IR instruments (Clarisse et al., 2013);

– to provide information in NRT on volcanic SO_2 plume height from satellite observations (e.g. Van Gent et al., 2013);

– to implement new visualisation tools and different levels of notification, in line with the users needs. In particular, customised notifications will be set-up to trigger volcanic plume dispersion modelling and forecasts as part of the ESA VAST project (http://vast.nilu.no).

Appendix A

Diagnosis of SACS from 2010 to 2012

For the period 2010–2012, we have investigated the success rate of SACS in detecting volcanic eruptions. We have listed all volcanic eruptions detected by the SACS warning system and compared them to the volcanoes known to be active for this period (80 in total), according to the Global Volcanism Programme (www.volcano.si.edu). The results can be found in Table 4, which gives the location of the 80 volcanoes and the corresponding SACS regions. The volcanoes in red correspond to the volcanoes for which SACS has detected volcanic activity. The detection scores by SACS are the following: 37 % in 2010, 62 % in 2011, and 71 % detected in 2012. Note that the criteria of volcanic activity considered by GVP is not only based on the emission of gas and particles in the atmosphere, as seismic activity plays a key role in their survey. From the SACS point of view and air traffic safety, all the strong eruptions with a threat to aviation have been detected. These results prove the quality of our system. For the year 2012, the SACS multi sensors system has issued 316 notifications with only 11 false notifications (success rate of 96 %).

Acknowledgements. Many thanks to ESA for the funding (SACS, SACS+ and SACS2 projects) and the support. We are grateful to NASA and FMI for the very fast delivery of OMI, CNES and EUMETSAT for data of IASI and GOME-2. We thank also JPL/NASA for the free access to AIRS data on EOSDIS. We would like also to acknowledge the team from the Toulouse VAAC (Météo-France), the London VAAC (UK-MetOffice), the Darwin VAAC (Bureau of Meteorology), the Anchorage VAAC (NOAA), the Wellington VAAC (MetService), the Montréal VAAC (Government of Canada), and all the users for their very useful feedback, which brings us energy and motivation and helps us to continue and to improve our service. This work was also undertaken under the auspices of the O3M SAF project of the EUMETSAT. P. F. Coheur and L. Clarisse are respectively Research Associate and Postdoctoral Researcher with F.R.S.-FNRS. The research in Belgium was funded by the F.R.S.-FNRS, the Belgian State Federal Office for Scientific, Technical and Cultural Affairs and the European Space Agency (ESA-Prodex arrangements C-4000103226). Financial support by the "Actions de Recherche Concertées" (Communauté Française de Belgique) is also acknowledged.

References

Aumann, H. H., Gregorich, D., Gaiser, S., Hagan, D., Pagano, T., Strow, L. L., and Ting, D.: AIRS Algorithm Theoretical Basis Basis Document, Level 1B, Part 1: Infrared Spectrometer, Version 2.2i, Jet Propulsion Laboratory, California Institute of technology, Pasadena, California, 10 November 2000.

Aumann, H. H., Chahine, M. T., Gautier, C., Goldberg, M. D., Kalnay, E., McMillin, L. M., Revercomb, H., Rosenkranz, P. W., Smith, W. L., Staelin, D. H., Strow, L. L., and Susskind, J.: AIRS/AMSU/HSB on the Aqua mission: design, science objectives, data products, and processing systems, IEEE T. Geosci. Remote, 41, 253–264, 2003.

Baxter, P. J., Bonadonna, C., Dupree, R., Hards, V. L., Kohn, S. C., Murphy, M. D., Nichols, A., Nicholson, R. A., Norton, G., Searl, A., Sparks, R. S. J., and Vickers, B. P.: Cristobalite in volcanic ash of the Soufriere Hills Volcano, Montserrat: hazards implications, Science, 283, 1142–1145, doi:10.1136/oem.59.8.523, 1999.

Bluth, G. J. S. and Carn, S. A.: Exceptional sulfur degassing from Nyamuragira volcano, 1979–2005, Int. J. Remote Sens., 29, 6667–6685, doi:10.1080/01431160802168434, 2008.

Bovensmann, H., Burrows, J. P., Buchwitz, M., Frerick, J., Noël, S., Rozanov, V. V., Chance, K. V., and Goede, A. P. H.: SCIAMACHY: mission objectives and measurement modes, J. Atmos. Sci., 56, 127–150, doi:10.1175/1520-0469(1999)056<0127:SMOAMM>2.0.CO;2, 1999.

Cantor, R.: Complete avoidance of volcanic ash is only procedure that guarantees flight safety, International Civil Aviation Organization Magazine (Int. Civil Aviation Org. Mag.), 53, 18–19, 1998.

Carn, S. A. and Lopez, T. M.: Opportunistic validation of sulfur dioxide in the Sarychev Peak volcanic eruption cloud, Atmos. Meas. Tech., 4, 1705–1712, doi:10.5194/amt-4-1705-2011, 2011.

Carn, S. A., Krueger, A. J., Krotkov, N. A., Arellano, S., and Yang, K.: Daily monitoring of Ecuadorian volcanic degassing from space, J. Volcanol. Geotherm. Res., 176, 141–150, doi:10.1016/j.jvolgeores.2008.01.029, 2008.

Casadevall, T. J.: The 1989/1990 eruption of Redoubt Volcano Alaska: impacts on aircraft operations, J. Volcanol. Geoth. Res., 62, 301–316, doi:10.1016/0377-0273(94)90038-8, 1994.

Casadevall, T. J., Delos Reyes, P. J., and Schneider, D. J.: The 1991 Pinatubo eruptions and their effects on aircraft operations, in: Fire and Mud: Eruptions and Lahars of Mount Pinatubo, Philippines, edited by: Newhall, C. G. and Punongbayan, R. S., Philippines Institute of Volcanology and Seismology, Quezon City, University of Washington Press, Seattle, 625–636, 1996.

Clarisse, L., Coheur, P. F., Prata, A. J., Hurtmans, D., Razavi, A., Phulpin, T., Hadji-Lazaro, J., and Clerbaux, C.: Tracking and quantifying volcanic SO_2 with IASI, the September 2007 eruption at Jebel at Tair, Atmos. Chem. Phys., 8, 7723–7734, doi:10.5194/acp-8-7723-2008, 2008.

Clarisse, L., Prata, F., Lacour, J.-L., Hurtmans, D., Clerbaux, C., and Coheur, P.-F.: A correlation method for volcanic ash detection using hyperspectral infrared measurements, Geophys. Res. Lett., 37, L19806, doi:10.1029/2010GL044828, 2010.

Clarisse, L., Coheur, P.-F., Chefdeville, S., Lacour, J. L., Hurtmans, D., and Clerbaux, C.: Infrared satellite observations of hydrogen sulfide in the volcanic plume of the August 2008 Kasatochi eruption, Geophys. Res. Lett., 398, L10804, doi:10.1029/2011GL047402, 2011.

Clarisse, L., Hurtmans, D., Clerbaux, C., Hadji-Lazaro, J., Ngadi, Y., and Coheur, P.-F.: Retrieval of sulphur dioxide from the infrared atmospheric sounding interferometer (IASI), Atmos. Meas. Tech., 5, 581–594, doi:10.5194/amt-5-581-2012, 2012.

Clarisse, L., Coheur, P.-F., Prata, F., Hadji-Lazaro, J., Hurtmans, D., and Clerbaux, C.: A unified approach to infrared aerosol remote sensing and type specification, Atmos. Chem. Phys., 13, 2195–2221, doi:10.5194/acp-13-2195-2013, 2013.

Clerbaux, C., Boynard, A., Clarisse, L., George, M., Hadji-Lazaro, J., Herbin, H., Hurtmans, D., Pommier, M., Razavi, A., Turquety, S., Wespes, C., and Coheur, P.-F.: Monitoring of atmospheric composition using the thermal infrared IASI/MetOp sounder, Atmos. Chem. Phys., 9, 6041–6054, doi:10.5194/acp-9-6041-2009, 2009.

Deroussi, S., Diament, M., Feret, J., Nebut, T., and Staudacher, T.: Localization of cavities in a thick lava flow by microgravimetry, J. Volcanol. Geotherm. Res., 184, 193–198, doi:10.1016/j.jvolgeores.2008.10.002, 2009.

Eckhardt, S., Prata, A. J., Seibert, P., Stebel, K., and Stohl, A.: Estimation of the vertical profile of sulfur dioxide injection into the atmosphere by a volcanic eruption using satellite column measurements and inverse transport modeling, Atmos. Chem. Phys., 8, 3881–3897, doi:10.5194/acp-8-3881-2008, 2008.

ESCAP: Review of developments in transport in Asia and the Pacific 2005, United Nations Publ., No. E.06.II.F.9, ST/ESCAP/2392, 172 pp., United Nations, New York, 2005.

Forbes, L., Jarvis, D., Potts, J., and Baxter, P. J.: Volcanic ash and respiratory symptoms in children on the island of Montserrat, British West Indies, Occup. Environ. Med., 60, 207–211, 2003.

Galle, B., Bobrowski, N., Carn, S., Durieux, J., Johansson, M., Kasereka, M., Oppenheimer, C., Yalire, M., and Zhang, Y.: Gas emissions from Nyiragongo volcano, D. R. of Congo, measured by UV mini-DOAS spectroscopy, Geophys. Res. Abstr., 7, EGU General Assembly, 9-2-2005, Vienna, Austria, 2005.

Geist, D. J., Harpp, K. S., Naumann, T. R., Poland, M., Chadwick, W. W., Hall, M., and Rader, E.: The 2005 eruption of Sierra Negra volcano, Galápagos, Ecuador, Bull. Volc., 70, 655–673, 2008.

Guffanti, M., Casadevall, T. J., and Budding, K.: Encounters of aircraft with volcanic ash clouds: a compilation of known incidents, 1953–2009, US Geological Data Series 545, ver. 1.0, 12 p., plus 4 appendixes including the compliation database, Technical Report, available at: http://pubs.usgs.gov/ds/545, last access: 13 January 2013, 2010.

NHESSD
1, 5935–6000, 2013

An online service for near real-time satellite monitoring of volcanic plumes

H. Brenot et al.

Haywood, J. M., Jones, A., Clarisse, L., Bourassa, A., Barnes, J., Telford, P., Bellouin, N., Boucher, O., Agnew, P., Clerbaux, C., Coheur, P.-F., Degenstein, D., and Braesicke, P.: Observations of the eruption of the Sarychev volcano and simulations using the HadGEM2 climate model, J. Geophys. Res., 115, D21212, doi:10.1029/2010JD014447, 2010.

Herman, J. R., Bhartia, P. K., Torres, O., Hsu, C., Seftor, C., and Celarier, E., Global distribution of UV-absorbing aerosols from Nimbus 7/TOMS data, J. Geophys. Res., 102, 16911–16922, doi:10.1029/96JD03680, 1997.

Hilton, F., Armante, R., August, T., Barnet, C., Bouchard, A., Camy-Peyret, C., Capelle, V., Clarisse, L., Clerbaux, C., Coheur, P.-F., Collard, A., Crevoisier, C., Dufour, G., Edwards, D., Faijan, F., Fourrié, N., Gambacorta, A., Goldberg, M., Guidard, V., Hurtmans, D., Illingworth, S., Jacquinet-Husson, N., Kerzenmacher, T., Klaes, D., Lavanant, L., Masiello, G., Matricardi, M., McNally, A., Newman, S., Pavelin, E., Payan, S., Péquignot, E., Peyridieu, S., Phulpin, T., Remedios, J., Schlüssel, P., Serio, C., Strow, L., Stubenrauch, C., Taylor, J., Tobin, D., Wolf, W., and Zhou, D.: Hyperspectral Earth Observation from IASI: four years of accomplishments, B. Am. Meteorol. Soc., 93, 347–370, 2012.

Hofstadter, M., Aumann, H. H., Manning, E., and Gaiser, S.: AIRS Algorithm Theoretical Basis Basis Document, Level 1B, Part 2: Visible/Near-Infrared Channels, Version 2.2, JPL D-17004, Jet Propulsion Laboratory, California Institute of technology, Pasadena, California, 10 November 2000.

IATA: Press Release: Volcano Crisis Cost Airlines $1.7 Billion in Revenue – IATA Urges Measures to Mitigate Impact, available at: http://www.iata.org/pressroom/pr/Pages/2010-04-21-01.aspx, last access: 2013, 2010.

ICAO: EUR DOC 9974 – Flight Safety and Volcanic Ash (Advance edition), International Civil Aviation Authority, available at: http://www.icao.int/publications/Documents/9974_unedited_en.pdf, last access: 2013, 2012.

Karagulian, F., Clarisse, L., Clerbaux, C., Prata, A. J., Hurtmans, D., and Coheur, P. F.: Detection of volcanic SO_2, ash, and H_2SO_4 using the Infrared Atmospheric Sounding Interferometer (IASI), J. Geophys. Res., 115, D00L02, doi:10.1029/2009JD012786, 2010.

Krotkov, N. A., Schoeberl, M. R., Morris, G. A., Carn, S. A., and Yang, K.: Dispersion and lifetime of the SO_2 cloud from the August 2008 Kasatochi eruption, J. Geophys. Res., 115, D00L20, doi:10.1029/2010JD013984, 2010.

NHESSD

1, 5935–6000, 2013

Levelt, P. F., van den Oord, G. H. J., Dobber, M. R., Mälkki, A., Visser, H., de Vries, J., Stammes, P., Lundell, J. O. V., and Saari, H.: The Ozone Monitoring Instrument, IEEE Trans. Geosci. Remote, 44, 1093–1101, doi:10.1109/TGRS.2006.872333, 2006.

Miller, T. P. and Casadevall, T. J.: Volcanic ash hazards to aviation, in: Encyclopedia of Volcanoes, edited by: Sigurdsson, H., Houghton, B., McNutt, S. R., Ryman, H., and Stix, J., Academic Press, San Diego, 915–930, 1999.

Munro, R., Eisinger, M., Anderson, C., Callies, J., Corpaccioli, E., Lang, R., Lefebvre, A., Livschitz, Y., and Albinana, A. P.: GOME-2 on MetOp, in: Proceedings of the 2006 EUMETSAT Meteorological Satellite Conference, Helsinki, Finland, 12–16 June 2006, EUMETSATP.48, 2006.

Oppenheimer, C., Scaillet, B., and Martin, R. S.: Sulfur degassing from volcanoes: source conditions, surveillance, plume chemistry and impacts, Rev. Mineral. Geochem., 73, 363–421, doi:10.2138/rmg.2011.73.13, 2011.

Platt, U. and J. Stutz, Differential Optical Absorption Spectroscopy: Principles and Applications, Springer Verlag, Heidelberg, ISBN 978-3540211938, 597 pp., 2008.

Prata, A. J.: Satellite detection of hazardous volcanic clouds and the risk to global air traffic: Nat. Hazards, 51, 303–324, doi:10.1007/s11069-008-9273-z, 2009.

Prata, A. J. and Bernardo, C.: Retrieval of volcanic SO_2 column abundance from Atmospheric Infrared Sounder data, J. Geophys. Res., 112, D20204, doi:10.1029/2006JD007955, 2007.

Prata, A. J., Carn, S. A., Stohl, A., and Kerkmann, J.: Long range transport and fate of a stratospheric volcanic cloud from Soufrière Hills volcano, Montserrat, Atmos. Chem. Phys., 7, 5093–5103, doi:10.5194/acp-7-5093-2007, 2007.

Prata, A. J., Gangale, G., Clarisse, L., and Karagulian, F.: Ash and sulfur dioxide in the 2008 eruptions of Okmok and Kasatochi: insights from high spectral resolution satellite measurements, J. Geophys. Res., 115, D00L18, doi:10.1029/2009JD013556, 2010.

Prata, A. J. and Prata, A. T.: Eyjafjallajökull volcanic ash concentrations determined using Spin Enhanced Visible and Infrared Imager measurements, J. Geophys. Res., 117, D00U23, doi:10.1029/2011JD016800, 2012.

Rix, M., Valks, P., Hao, N., Van Geffen, J., Clerbaux, C., Clarisse, L., Coheur, P.-F., Loyola, D., Erbertseder, T., Zimmer, W., and Emmadi, S.: Satellite monitoring of volcanic sulfur dioxide emissions for early warning of volcanic hazards, IEEE Journal of Selected Topics in Applied Earth Observations and Remote Sensing, 2, 196–206, doi:10.1109/JSTARS.2009.2031120, 2009.

Rix, M., Valks, P., Hao, N., Loyola, D. G., Schlager, H., Huntrieser, H. H., Flemming, J., Koehler, U., Schumann, U., and Inness, A.: Volcanic SO_2, BrO and plume height estimations using GOME-2 satellite measurements during the eruption of Eyjafjallajökull in May 2010, J. Geophys. Res., 117, D00U19, doi:10.1029/2011JD016718, 2012.

Robock, A.: Volcanic eruptions and climate, Rev. Geophys., 38, 191–219, doi:10.1029/1998RG000054, 2000.

Robock, A. and Oppenheimer, C. (Eds.): Volcanism and the Earth's Atmosphere, Geophys. Monogr. Ser., 139, AGU, Washington DC, doi:10.1029/GM139, 360 pp., 2003.

Stohl, A., Prata, A. J., Eckhardt, S., Clarisse, L., Durant, A., Henne, S., Kristiansen, N. I., Minikin, A., Schumann, U., Seibert, P., Stebel, K., Thomas, H. E., Thorsteinsson, T., Tørseth, K., and Weinzierl, B.: Determination of time- and height-resolved volcanic ash emissions and their use for quantitative ash dispersion modeling: the 2010 Eyjafjallajökull eruption, Atmos. Chem. Phys., 11, 4333–4351, doi:10.5194/acp-11-4333-2011, 2011.

Surono, Jousset, P., Pallister, J., Boichu, M., Buongiorno, M., Budisantoso, A., Costa, F., Andreastuti, S., Prata, F., Schneider, D., Clarisse, L., Humaida, H., Sumarti, S., Bignami, C., Griswold, J., Carn, S., Oppenheimer, C., and Lavigne, F.: The 2010 explosive eruption of Javas Merapi volcano – a "100 years" event, J. Volcanol. Geoth. Res., 241–242, 121–135, doi:10.1016/j.jvolgeores.2012.06.018, 2012.

Thomas, H. E. and Prata, A. J.: Sulphur dioxide as a volcanic ash proxy during the April–May 2010 eruption of Eyjafjallajökull Volcano, Iceland, Atmos. Chem. Phys., 11, 6871–6880, doi:10.5194/acp-11-6871-2011, 2011.

Thomas, H. I. and Watson, I. M.: Observations of volcanic emissions from space: current and future perspectives, Nat. Hazards, 54, 323–354, 2010.

Torres, O., Bhartia, P. K., Herman, J. R., Ahmad, Z., and Gleason, J.: Derivation of aerosol properties from satellite measurements of backscattered ultraviolet radiation, theoretical basis, J. Geophys. Res., 103, 17099–17110, 1998.

Tulet, P. and Villeneuve, N.: Large scale modeling of the transport, chemical transformation and mass budget of the sulfur emitted during the April 2007 eruption of Piton de la Fournaise, Atmos. Chem. Phys., 11, 4533–4546, doi:10.5194/acp-11-4533-2011, 2011.

Van Geffen, J., Van Roozendael, M., Di Nicolantonio, W., Tampellini, L., Valks, P., Erbetseder, T., and Van der A, R.: Monitoring of volcanic activity from satellite as part of GSE PROMOTE, in: Proceedings of the 2007 Envisat Symposium, ESA, Montreux, Switzerland, 23–27 April 2007, publication SP-636, 23–27, 2007.

NHESSD

1, 5935–6000, 2013

Van Geffen, J., Van Roozendael, M., Rix, M., and Valks, P.: Initial validation of GOME-2 GDP 4.2 SO_2 total columns (OTO/SO2) – ORR B, O3MSAF validation report, TN-IASB-GOME2-O3MSAF-SO2-01.1, Darmstadt, Germany, EUMETSAT, 2008.
Van Gent, J., Spurr, R., Theys, N., Lerot, C., Brenot, H., Dils, B., and Van Roozendael, M.: Towards an operational SO_2 plume altitude algorithm for GOME-2 radiance measurements, Atmos. Meas. Tech. Discuss., in preparation, 2013.
Yan, H., Chen, L., Tao, J., Su, L., Huang, J., Han, D., and Yu, C.: Corrections for OMI SO_2 BRD retrievals influenced by row anomalies, Atmos. Meas. Tech., 5, 2635–2646, doi:10.5194/amt-5-2635-2012, 2012.
Yang, K., Krotkov, N. A., Krueger, A. J., Carn, S. A., Bhartia, P. K., and Levelt, P. F.: Retrieval of large volcanic SO_2 columns from the Aura Ozone Monitoring Instrument (OMI): comparison and limitations, J. Geophys. Res., 112, D24S43, doi:10.1029/2007JD008825, 2007.
Yang, K., Liu, X., Krotkov, N. A., Krueger, A. J., and Carn, S. A.: Estimating the altitude of volcanic sulfur dioxide plumes from space borne hyper-spectral UV measurements, Geophys. Res. Lett., 36, L10803, doi:10.1029/2009GL038025, 2009.
Witham, C. S., Hort, M. C., Potts, R., Servranckx, R., Husson, P., and Bonnardot, F.: Comparison of VAAC atmospheric dispersion models using the 1 November 2004 Grimsvötn eruption, Meteorol. Appl., 14, 27–38, doi:10.1002/met.3, 2007.
Zehner, C. (Ed.): Monitoring Volcanic Ash from Space, in: Proceedings of the ESA-EUMETSAT workshop on the 14 April to 23 May 2010 eruption at the Eyjafjoll volcano, South Iceland, Frascati, Italy, 26–27 May 2010, ESA-Publication STM-280, doi:10.5270/atmch-10-01, 2010.

NHESSD
1, 5935–6000, 2013

An online service for near real-time satellite monitoring of volcanic plumes

H. Brenot et al.

NHESSD
1, 5935–6000, 2013

An online service for near real-time satellite monitoring of volcanic plumes

H. Brenot et al.

Table 1. List of data products available from SACS.

Instruments	Data type	Overpass time	Data availability	Resolution (km^2)	Swath (km)	Global coverage (h)	Data products	Participants	Units	Delay
SCIAMACHY (ENVISAT)	UV/visible	10:00 a.m.	Apr 2004–2012	30 × 60	960	96	SO_2 vertical columns Absorbing aerosol index	BIRA KNMI	DU –	2–3 h 2–3 h
OMI (Aura)	UV/visible	01:30 p.m.	Sep 2004–present	13 × 24	2600	24	SO_2 vertical columns Absorbing aerosol index	NASA/KNMI/FMI KNMI	DU –	2–3 h (EU: 45') 2–3 h
GOME-2 (MetOp-A)	UV/visible	09:30 a.m.	Jan 2007–present	40 × 80	1920	24	SO_2 vertical columns SO_2 plume height Absorbing aerosol index	DLR BIRA KNMI	DU km –	1–2 h off-line 2–3 h
IASI (MetOp-A)	Infrared	09:30 a.m. 09:30 p.m.	Oct 2007–present	12 × 12	2200	12	SO_2 index (and columns) Ash indicator	ULB ULB	K (DU) –	1–2 h 1–2 h
AIRS (Aqua)	Infrared	01:30 a.m. 01:30 p.m.	Sep 2002–present	15 × 15	1650	12	SO_2 vertical columns Ash indicator	NILU ULB	DU –	1–2 h 1–2 h

Table 2. Geographical coverage of SACS monitoring for October 2012.

Zone	Duration of monitoring: 1 h		2 h		3 h		4 h		6 h		8 h		12 h		24 h	
	Pixel	(max)	Pixel	(max)	Pixel	(max)	Pixel	(max)	Pixel	(max)	Pixel	(max)	Pixel	(max)	Pixel	(max)
A	14.5 %	(5)	28.8 %	(5)	42.5 %	(5)	55.0 %	(7)	75.0 %	(8)	88.5 %	(8)	98.0 %	(8)	100 %	(13)
B	15.9 %	(5)	31.2 %	(5)	46.0 %	(6)	59.0 %	(7)	78.5 %	(8)	90.9 %	(8)	98.5 %	(9)	100 %	(15)
C	18.8 %	(5)	36.1 %	(7)	51.3 %	(8)	64.8 %	(9)	84.9 %	(10)	97.0 %	(10)	99.7 %	(11)	100 %	(17)
D	24.7 %	(7)	44.8 %	(9)	57.9 %	(11)	71.0 %	(12)	90.3 %	(13)	99.8 %	(14)	100 %	(15)	100 %	(23)
E	31.3 %	(8)	50.1 %	(10)	61.9 %	(14)	72.5 %	(19)	87.9 %	(22)	96.0 %	(30)	99.4 %	(38)	100 %	(71)
F	72.5 %	(8)	94.8 %	(10)	97.3 %	(14)	98.8 %	(19)	100.0 %	(22)	100 %	(30)	100 %	(38)	100 %	(71)
World	31.6 %	(8)	50.6 %	(10)	62.3 %	(14)	72.8 %	(19)	88.1 %	(22)	96.1 %	(30)	99.4 %	(38)	100 %	(71)

Discussion Paper | Discussion Paper | Discussion Paper | Discussion Paper |

NHESSD
1, 5935–6000, 2013

An online service for near real-time satellite monitoring of volcanic plumes

H. Brenot et al.

Table 3. Key criteria used by the SACS SO_2 notification system.

Instruments	SCIAMACHY	GOME-2	OMI	IASI	AIRS
Threshold radius	80 km	85 km	50 km	No need	No need
Type of observation	VCD	VCD	VCD	DBT	VCD
Threshold values	1.8 DU	1.8 DU	1.45 DU	2.9 K	3 DU
Threshold value proximity volcano (< 300 km)	1.25 DU	1.45 DU	1.25 DU	No need	No need
Avoid SAA threshold value	Yes 3.25 DU	Yes 2 DU	No need	No need	No need
Avoid pollution threshold value	Yes 3.25 DU	Yes 2 DU	Yes 1.6 DU	No need	No need

NHESSD
1, 5935–6000, 2013

Table 4. List of the volcanoes having their last eruptions in years 2010, 2011 or 2012. The corresponding SACS region of these volcanoes, their positions (latitude, longitude and the altitude of the summit) are presented. The red band corresponds to the volcanoes for which SACS system has identified an SO_2 notifications.

SACS region	Longitude (°)	Latitude (°)	Summit (m)	Year	Volcano name
106	−19.62	63.63	1666	2010	Eyjafjallalökull
111	156.02	50.68	1156	2010	Ebeko
111	158.03	52.56	1829	2010	Gorely
111	153.93	48.96	1170	2010	Ekarma
203	−84.70	10.46	1670	2010	Arenal
203	−90.60	14.38	2552	2010	Pacaya
210	139.53	34.08	815	2010	Miyake-jima
210	123.68	13.26	2462	2010	Mayon
211	145.80	18.13	570	2010	Pagan
211	144.77	14.60	−517	2010	NW Rota-1
211	141.49	24.28	−14	2010	Fukutoku-Okanoba
303	−77.37	1.22	4276	2010	Galeras
307	35.91	−2.76	2962	2010	Ol Doinyo Lengai
310	123.58	−7.79	748	2010	Batu Tara
310	116.57	−8.42	3726	2010	Rinjani
311	148.42	−5.53	1330	2010	Langila
311	167.50	−14.27	797	2010	Gaua
404	−72.65	−42.83	1122	2010	Chaitén
408	55.71	−21.23	2632	2010	Piton de la Fournaise
101	−169.94	52.83	1730	2011	Cleveland
106	−17.33	64.42	1725	2011	Grímsvötn
106	−19.05	63.63	1512	2011	Katla
111	160.64	56.06	4835	2011	Kliuchevskoi
111	160.32	55.13	2376	2011	Kizimen

Discussion Paper | Discussion Paper | Discussion Paper | Discussion Paper |

NHESSD
1, 5935–6000, 2013

An online service for near real-time satellite monitoring of volcanic plumes

H. Brenot et al.

Table 4. Continued.

SACS region	Longitude (°)	Latitude (°)	Summit (m)	Year	Volcano name
203	−87.00	12.70	1745	2011	San Cristóbal
203	−85.62	11.54	1610	2011	Concepción
203	−86.85	12.60	1061	2011	Telica
209	93.86	12.28	354	2011	Barren Island
210	130.86	31.93	1700	2011	Kirishima
210	124.05	12.77	1565	2011	Bulusan
210	131.11	32.88	1592	2011	Aso
303	−77.66	−0.08	3562	2011	Reventador
307	41.70	13.37	2218	2011	Nabro
310	125.40	2.78	1827	2011	Karangetang [Api Siau]
310	124.73	1.11	1784	2011	Soputan
310	110.44	−7.54	2968	2011	Merapi
310	112.95	−7.94	2329	2011	Tengger Caldera
311	152.20	−4.27	688	2011	Rabaul
311	145.04	−4.08	1807	2011	Manam
311	151.33	−5.05	2334	2011	Ulawun
311	167.83	−15.40	1496	2011	Aoba
312	−175.07	−19.75	515	2011	Tofua
403	−70.57	−35.24	4107	2011	Planchón-Peteroa
403	−72.12	−40.59	2236	2011	Puyehue-Cordon Caulle
512	167.17	−77.53	3794	2011	Erebus
111	161.36	56.65	3283	2012	Shiveluch
111	159.45	54.05	1536	2012	Karymsky
111	160.59	55.98	2882	2012	Bezymianny
111	160.33	55.83	3682	2012	Tolbachik
201	−155.29	19.42	1222	2012	Kilauea
203	−103.62	19.51	3850	2012	Colima
203	−84.23	10.20	2708	2012	Poás

NHESSD
1, 5935–6000, 2013

Table 4. Continued.

SACS region	Longitude (°)	Latitude (°)	Summit (m)	Year	Volcano name
203	−90.88	14.47	3763	2012	Fuego
203	−91.55	14.76	3772	2012	Santa Maria
203	−98.62	19.02	5426	2012	Popocatépetl
203	−83.77	10.02	3340	2012	Turrialba
204	−62.18	16.72	915	2012	Soufrière Hills
206	15.21	38.79	924	2012	Stromboli
206	15.00	37.73	3330	2012	Etna
207	40.67	13.60	613	2012	Erta Ale
210	130.66	31.58	1117	2012	Sakura-jima
210	129.72	29.64	799	2012	Suwanose-jima
303	−75.32	4.89	5321	2012	Nevado del Ruiz
303	−78.34	−2.00	5230	2012	Sangay
303	−78.44	−1.47	5023	2012	Tungurahua
303	−76.03	2.93	5364	2012	Nevado del Huila
307	29.25	−1.52	3470	2012	Nyiragongo
307	29.20	−1.41	3058	2012	Nyamuragira
309	100.47	−0.38	2891	2012	Marapi
310	127.63	1.49	1325	2012	Ibu
310	127.88	1.68	1335	2012	Dukono
310	112.92	−8.11	3676	2012	Semeru
310	105.42	−6.10	813	2012	Krakatau
310	124.79	1.36	1580	2012	Lokon-Empung
311	155.20	−6.14	1750	2012	Bagana
404	−71.93	−39.42	2847	2012	Villarrica
404	−71.17	−37.85	2997	2012	Copahue
412	169.44	−19.53	361	2012	Yasur
412	168.12	−16.25	1334	2012	Ambrym
412	165.80	−10.38	851	2012	Tinakula

NHESSD
1, 5935–6000, 2013

Fig. 1. Illustration of the satellite equatorial overpasses (solar local time).

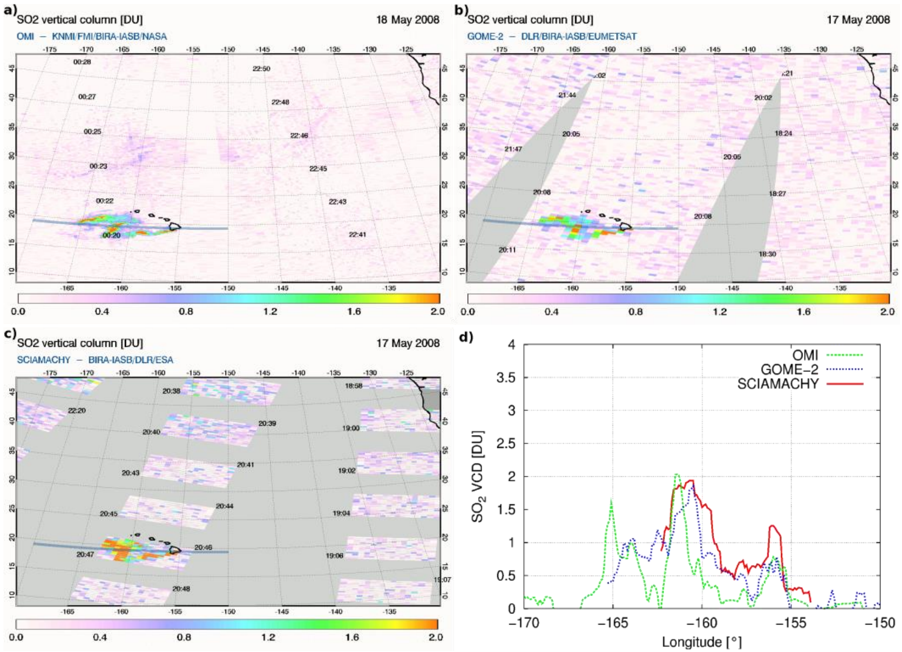

Fig. 2. SO_2VCD images by respectively **(a)** OMI, **(b)** GOME-2 and **(c)** SCIAMACHY. The lower right plot **(d)** shows the SO_2 VCDs for a fixed latitude of 19.4° N (blue line in the SO_2 images) as a function of longitude during an eruption of Kilauea volcano (155.29° W; 19.42° N), 17–18 May 2008.

NHESSD
1, 5935–6000, 2013

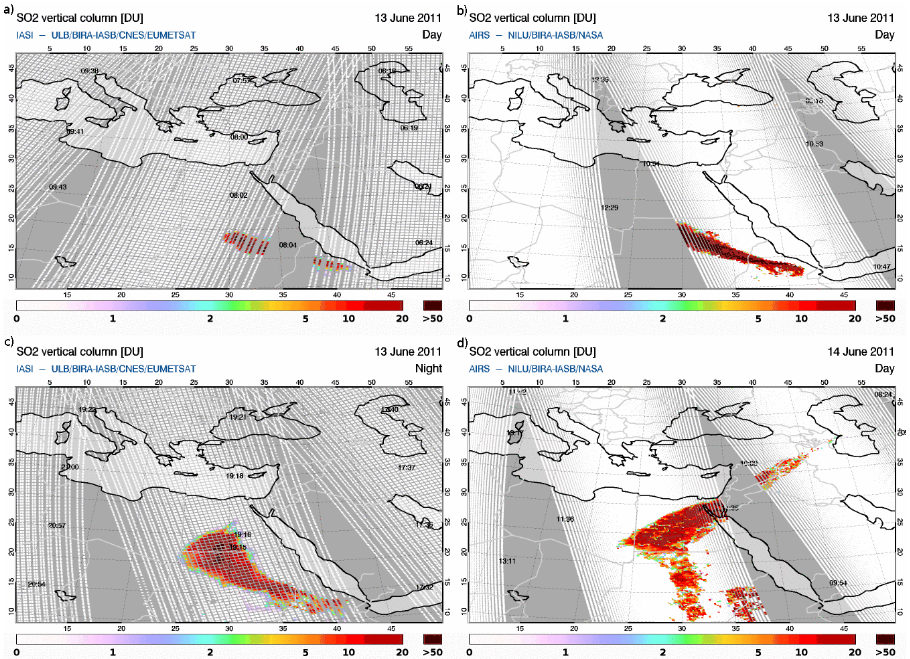

Fig. 3. SACS SO_2 vertical column density images from IASI and AIRS for the 13 and 14 June 2011 at the beginning of the eruption of Nabro. Note that IASI and AIRS observations are plotted using circles with mean diameters of respectively 12 km and 15 km.

NHESSD
1, 5935–6000, 2013

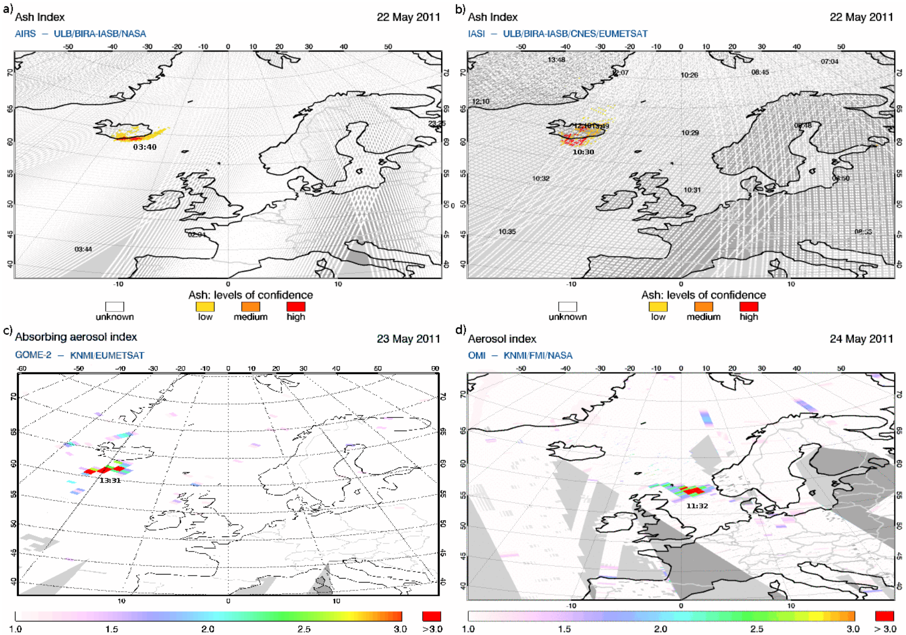

Fig. 4. Ash index from **(a)** IASI and **(b)** AIRS and AAI from **(c)** GOME-2 and **(d)** OMI during the Grímsvötn eruption on Iceland. Images show the first days of the eruption, which started on the afternoon of 21 May 2011.

NHESSD
1, 5935–6000, 2013

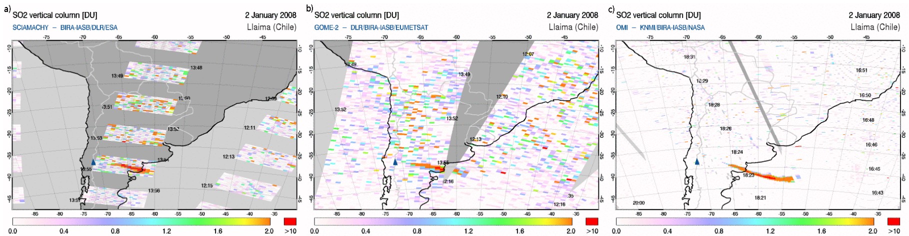

Fig. 5. Example of SO_2 VCD from **(a)** SCIAMACHY, **(b)** GOME-2, and **(c)** OMI on 2 January 2008 in the region affected by the SAA. The SO_2 plume is related to the eruption of the Llaima volcano (Chile), marked by a blue triangle in the plots. Artefacts in the SO_2 VCD from SCIAMACHY and GOME-2 instruments induced by the South Atlantic Anomaly are visible on these images; OMI is less affected.

NHESSD
1, 5935–6000, 2013

Title Page
Abstract | Introduction
Conclusions | References
Tables | Figures
◂ | ▸
Back | Close
Full Screen / Esc
Printer-friendly Version
Interactive Discussion

NHESSD
1, 5935–6000, 2013

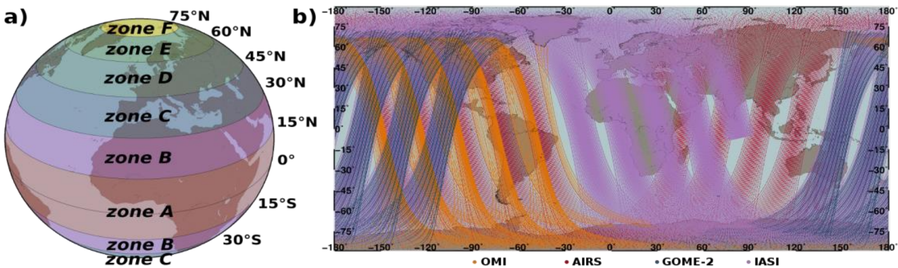

Fig. 6. (a) Geographical zones used in Table 2; **(b)** 8 h of monitoring from SACS instruments (example of 27 October 2012).

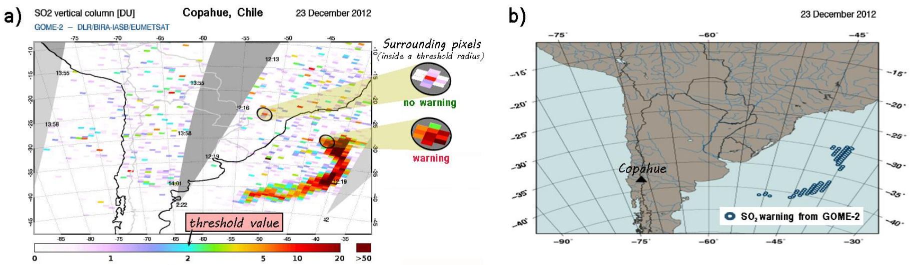

Fig. 7. Eruption of the Copahue volcano 23 December 2012. **(a)** SO_2 vertical column density from GOME-2. A zoom for two pixels above the "threshold value" is shown with the issues of warning. The black ellipse represents the area defined by the "threshold radius" considered in the SACS warning system (see Table 3); **(b)** locations of SO_2 warnings pixels.

NHESSD
1, 5935–6000, 2013

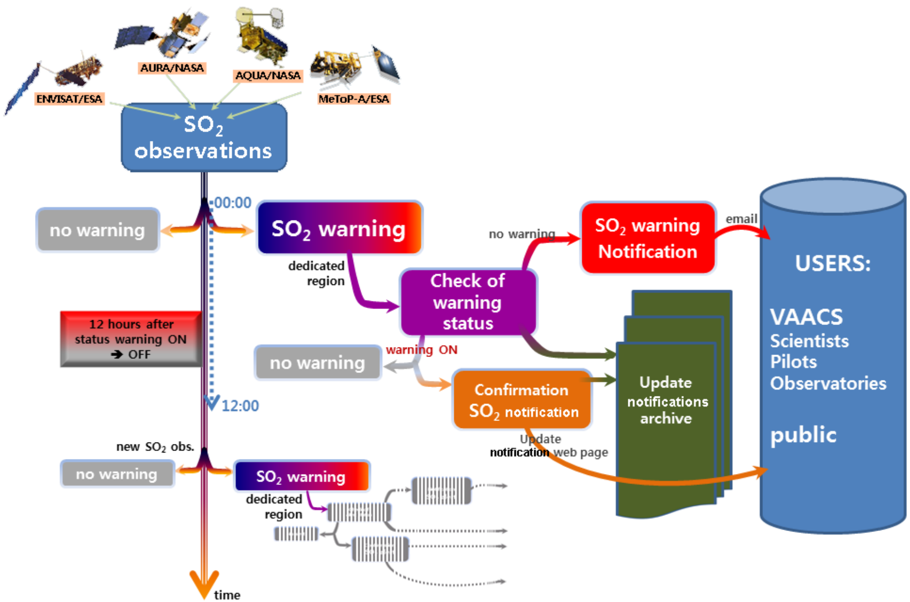

Fig. 8. Overview of the SACS notification system.

NHESSD
1, 5935–6000, 2013

An online service for near real-time satellite monitoring of volcanic plumes

H. Brenot et al.

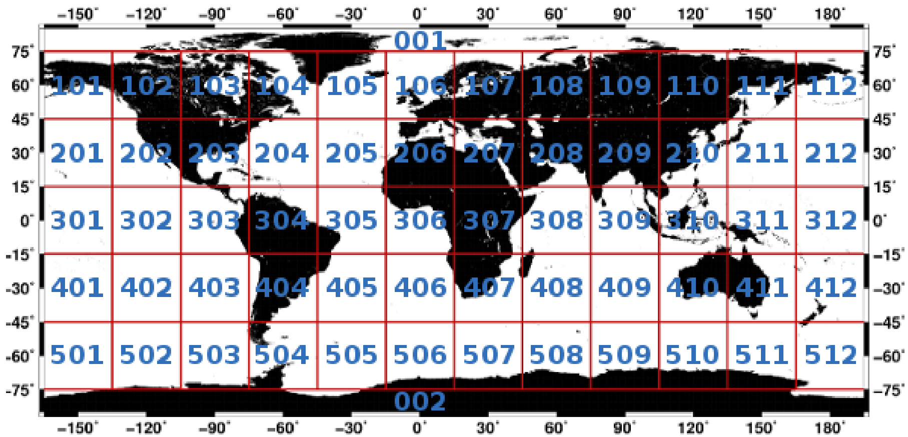

Fig. 9. Predefined world regions used by the SACS notification system and for the SO_2 monitoring service.

NHESSD
1, 5935–6000, 2013

An online service for near real-time satellite monitoring of volcanic plumes

H. Brenot et al.

Title Page
Abstract Introduction
Conclusions References
Tables Figures
◀I ▶I
◀ ▶
Back Close
Full Screen / Esc
Printer-friendly Version
Interactive Discussion

From SACS <sacs@aeronomie.be>
Subject **SACS warning -- GOME 2 -- 2012/09/01 23:42 -- region 112**
To SACS users

```
SACS multi-sensor warning of exceptional SO2 concentration
=========================================================
Process date : 2012/09/01
Process time : 23:42 UTC
Instrument   : GOME2

Warning region: 112
--------------------
http://sacs.aeronomie.be/GOME2alert/2012/09/alertsGOME2_20120901_22h41_112.php?alert=20120901_234250_112

Date         :    2012/09/01
Time         :    22:41  UTC
Longitude    :     167.7  deg.
Latitude     :     54.5  deg.
SZA          :     52.8  deg.
Max. SO2 vcd :     2.9   DU
Cloud data   :    used for VCD
```

Fig. 10. Example of an email notification sent to users in case of an exceptional SO_2 concentration detected.

NHESSD
1, 5935–6000, 2013

An online service for near real-time satellite monitoring of volcanic plumes

H. Brenot et al.

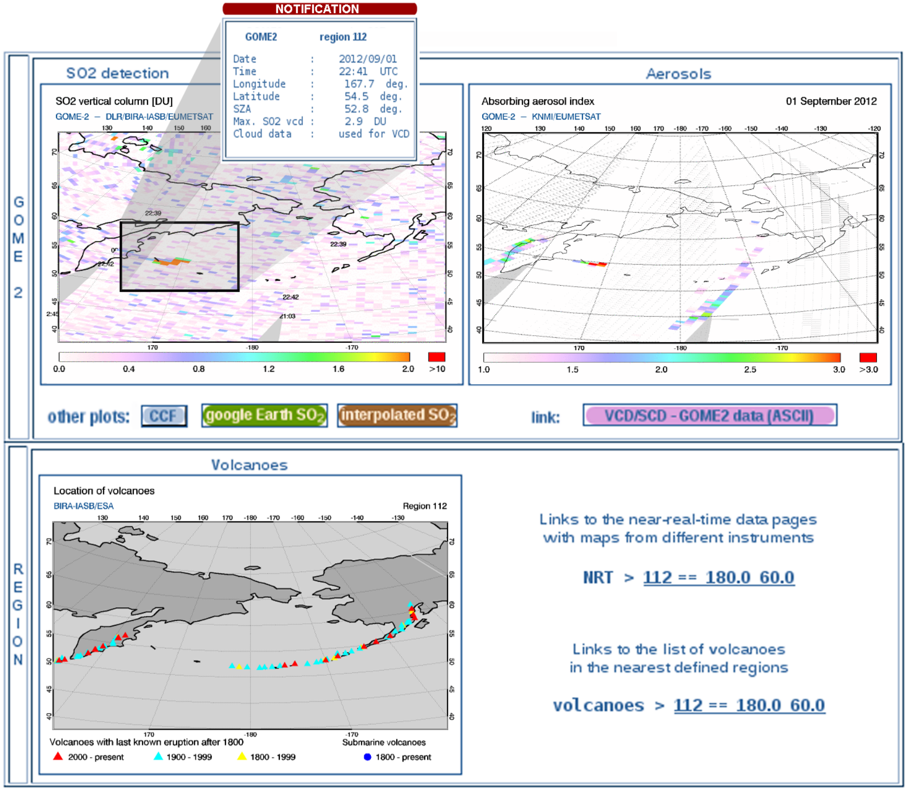

Fig. 11. SO_2 and aerosol images from GOME-2 (notification web page), on 1 September 2012 (eruption of the Bezymianny volcano in the Kuril islands).

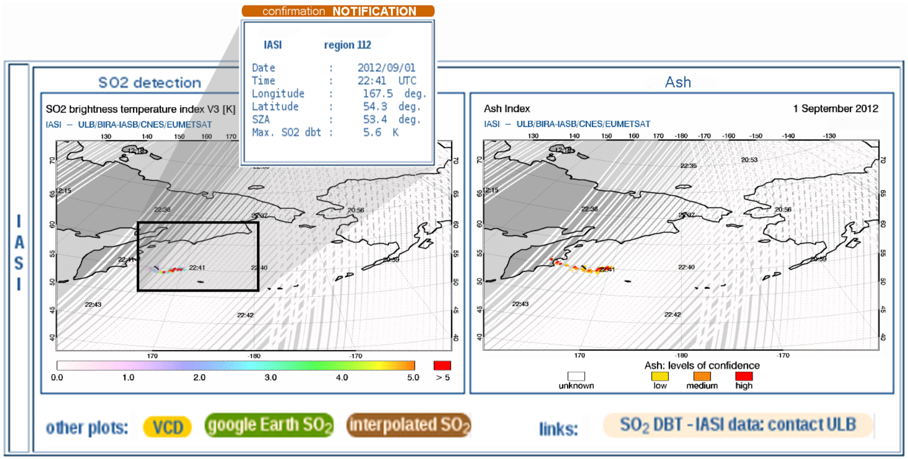

Fig. 12. SO_2 and ash images from IASI, on 1 September 2012. Confirmation of notification by IASI.

NHESSD
1, 5935–6000, 2013

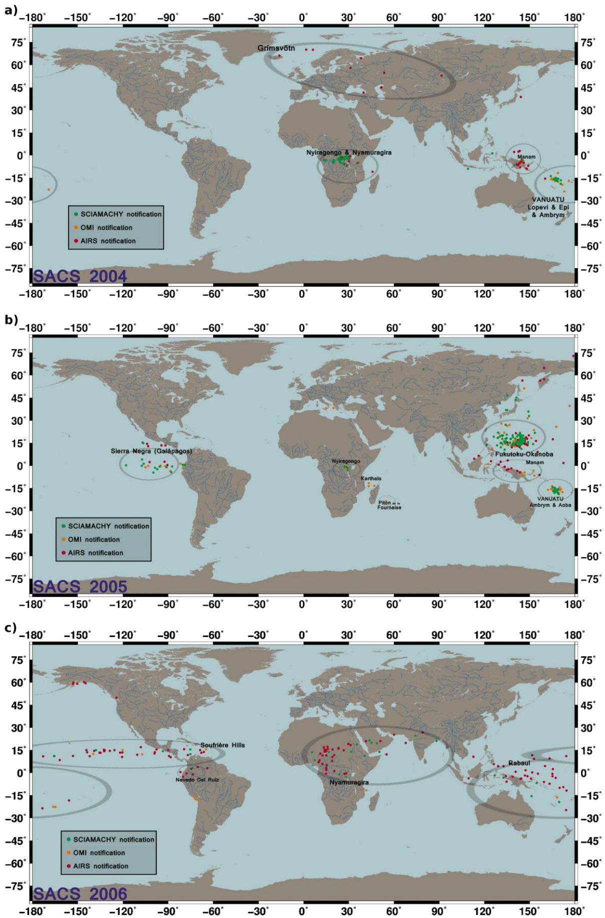

Fig. 13. SACS notifications for 2004, 2005, and 2006.

NHESSD
1, 5935–6000, 2013

An online service for near real-time satellite monitoring of volcanic plumes

H. Brenot et al.

Title Page
Abstract | Introduction
Conclusions | References
Tables | Figures
◀| |▶
◀ ▶
Back | Close
Full Screen / Esc
Printer-friendly Version
Interactive Discussion

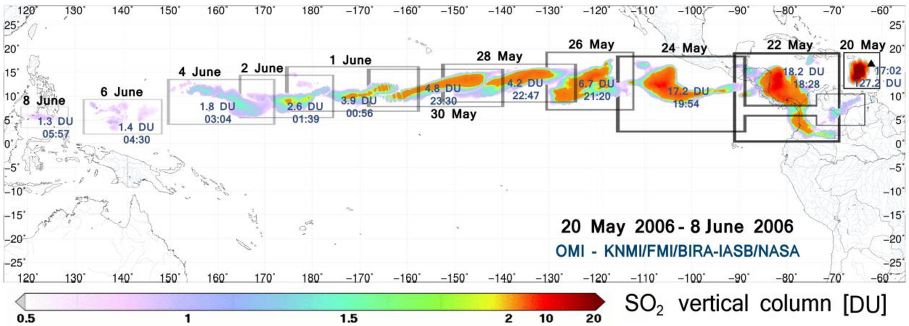

Fig. 14. OMI images of SO_2 emitted by Soufrière Hills volcano from 20 May to 8 June 2006 (from right to left).

NHESSD
1, 5935–6000, 2013

An online service for near real-time satellite monitoring of volcanic plumes

H. Brenot et al.

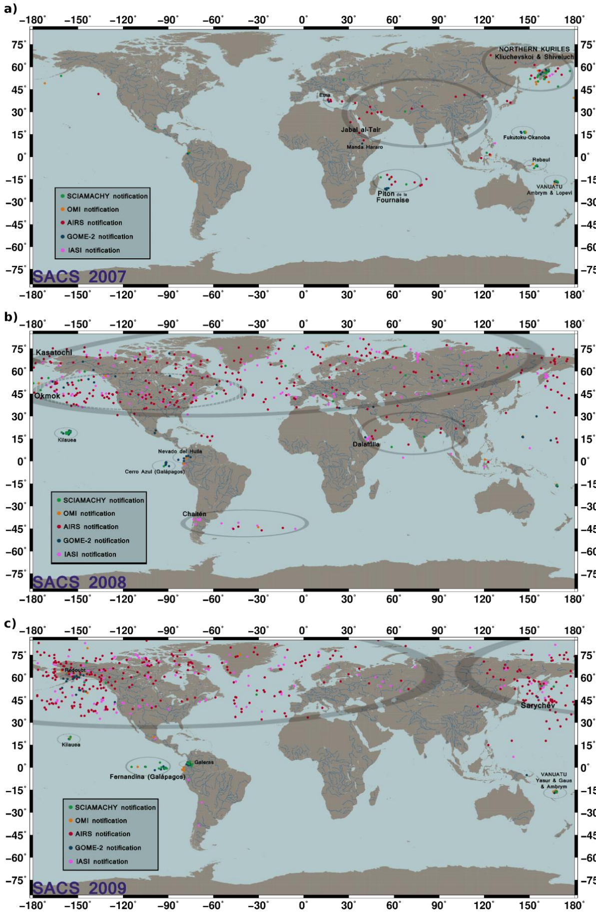

Fig. 15. SACS notifications for 2007, 2008, and 2009.

NHESSD
1, 5935–6000, 2013

An online service for near real-time satellite monitoring of volcanic plumes

H. Brenot et al.

Title Page
Abstract | Introduction
Conclusions | References
Tables | Figures
◀| |▶
◀ ▶
Back | Close
Full Screen / Esc
Printer-friendly Version
Interactive Discussion

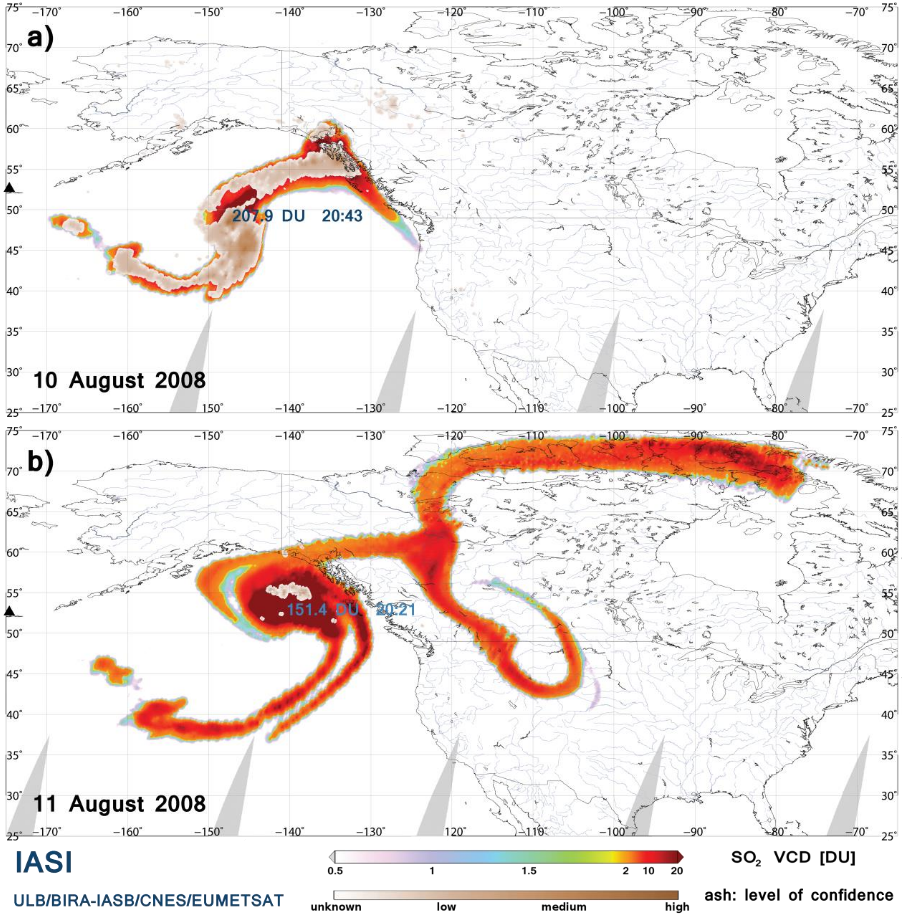

Fig. 16. IASI SO_2 column density and ash index emitted by the Kasatochi volcano on **(a)** 10 August 2008; **(b)** 11 August 2008.

NHESSD
1, 5935–6000, 2013

Title Page
Abstract Introduction
Conclusions References
Tables Figures
◀ ▶
Back Close
Full Screen / Esc
Printer-friendly Version
Interactive Discussion

NHESSD
1, 5935–6000, 2013

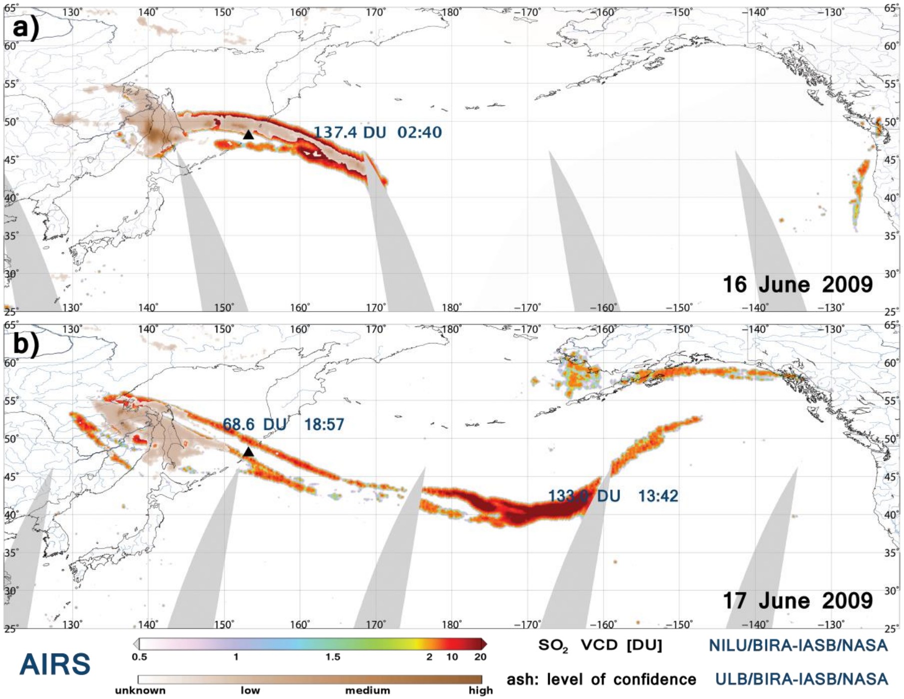

Fig. 17. AIRS SO_2 column density and ash index emitted by the Sarychev volcano on **(a)** 16 June 2009; **(b)** 17 June 2009.

Title Page
Abstract | Introduction
Conclusions | References
Tables | Figures
◀| |▶
◀ ▶
Back | Close
Full Screen / Esc
Printer-friendly Version
Interactive Discussion

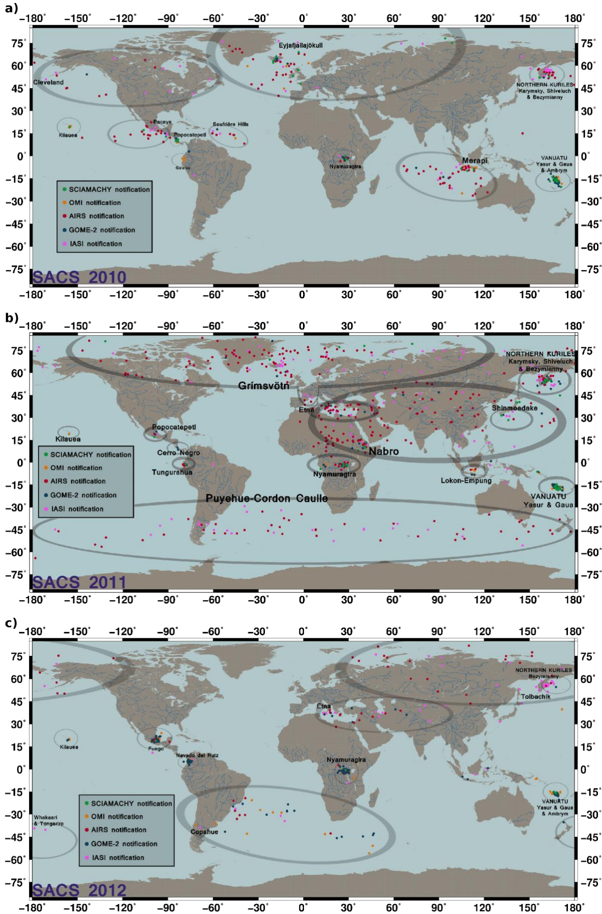

Fig. 18. SACS notifications for 2010, 2011, and 2012

NHESSD
1, 5935–6000, 2013

An online service for near real-time satellite monitoring of volcanic plumes

H. Brenot et al.

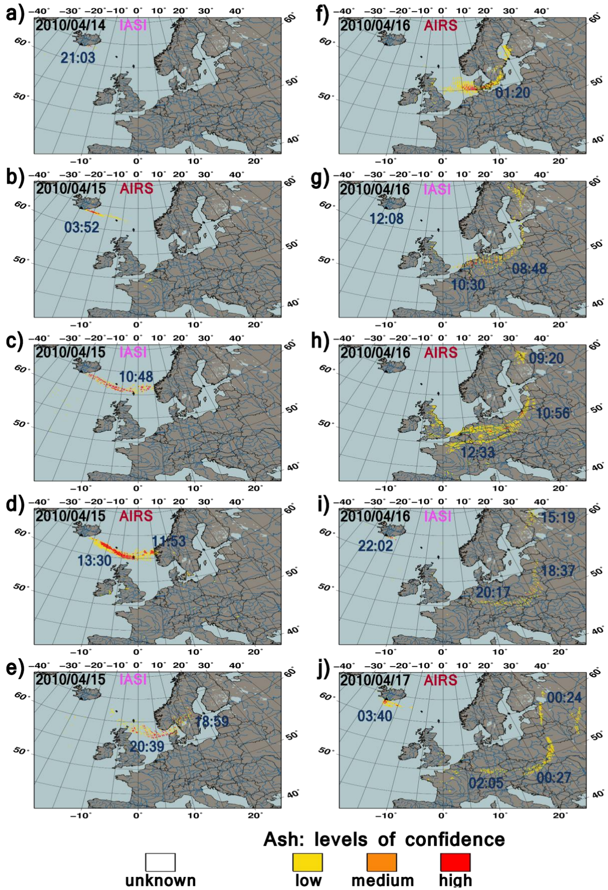

Fig. 19. Ash index images from thermal IR sensors (AIRS and IASI) during the eruption of Eyjafjallajökull volcano (Iceland) in spring 2010.

NHESSD

1, 5935–6000, 2013

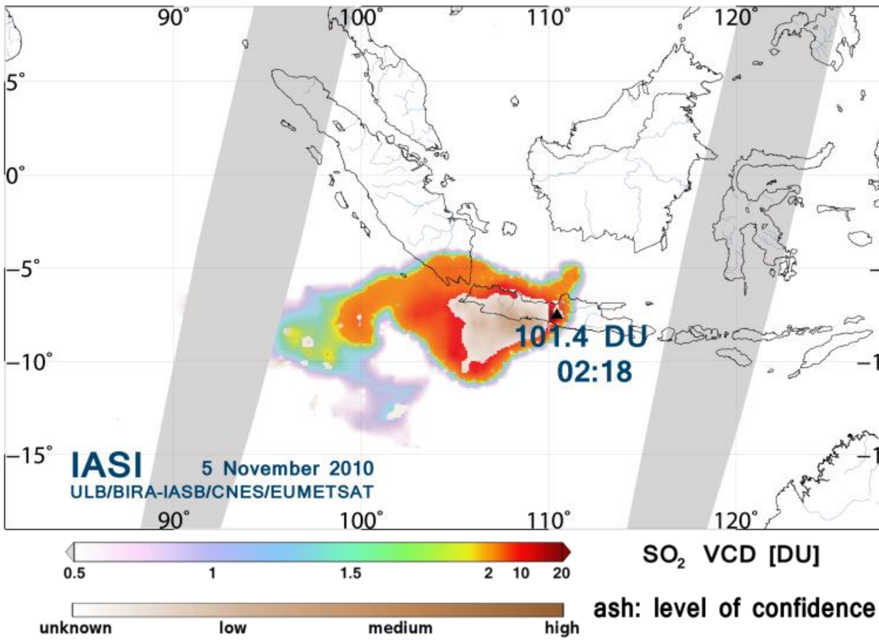

Fig. 20. Ash image superimposed over the SO_2 image from IASI during the Merapi's eruption (5 November 2010).

NHESSD
1, 5935–6000, 2013

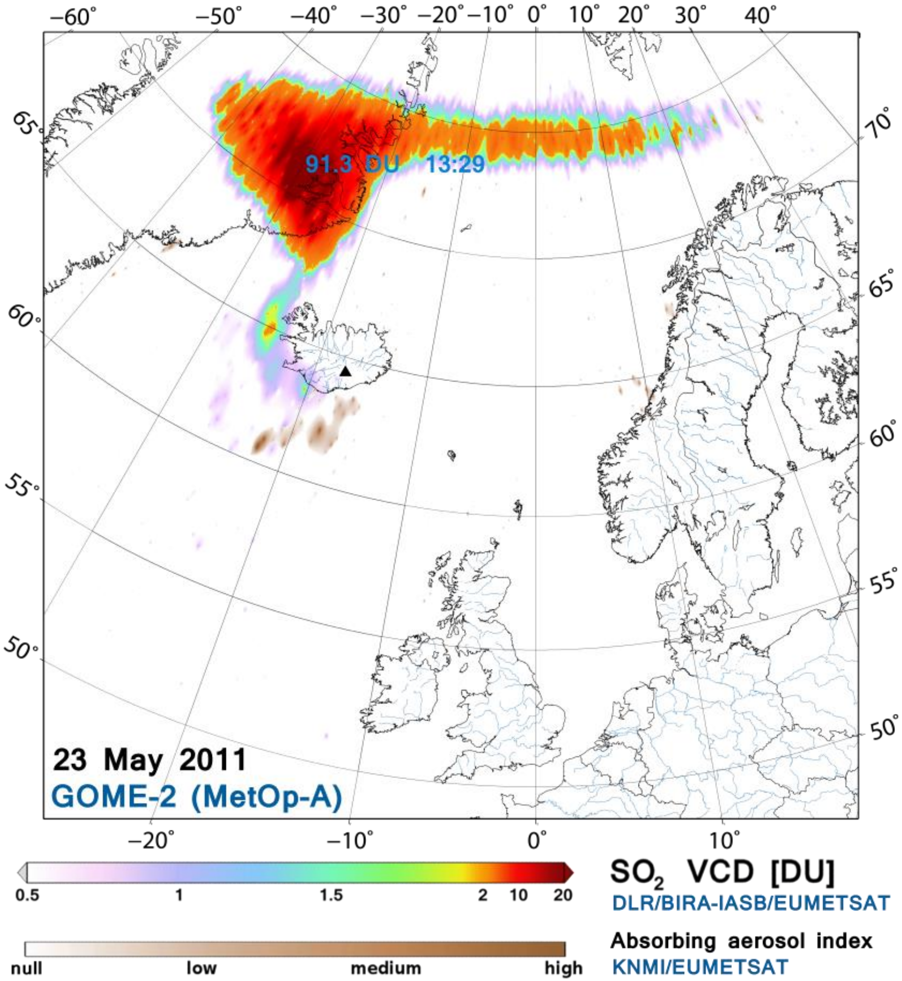

Fig. 21. SO_2 and aerosols (ash) detected by GOME-2 (Grìmsvötn eruption, 23 May 2011).

NHESSD
1, 5935–6000, 2013

Title Page
Abstract | Introduction
Conclusions | References
Tables | Figures
◀| |▶
◀ ▶
Back | Close
Full Screen / Esc
Printer-friendly Version
Interactive Discussion

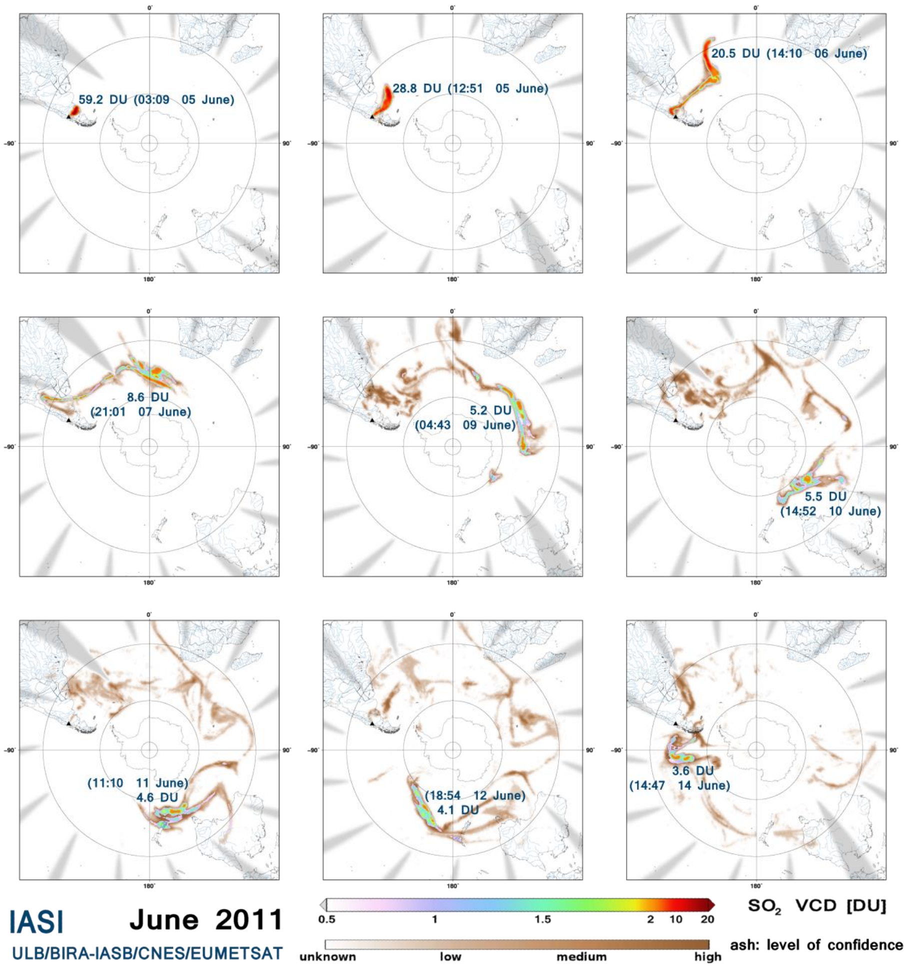

Fig. 22. SO_2 and ash detected by IASI (Puyehue-Cordón Caulle eruption, 6 June 2011).

NHESSD
1, 5935–6000, 2013

An online service for near real-time satellite monitoring of volcanic plumes

H. Brenot et al.

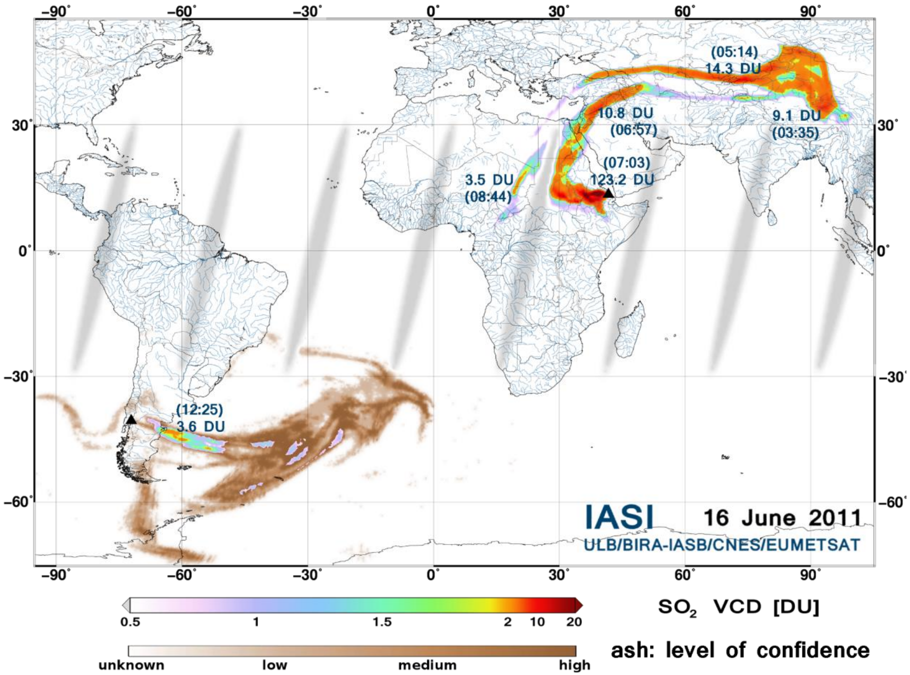

Fig. 23. SO_2 and ash detected by IASI (Nabro and Puyehue eruptions, 16 June 2011).

NHESSD
1, 5935–6000, 2013

An online service for near real-time satellite monitoring of volcanic plumes

H. Brenot et al.

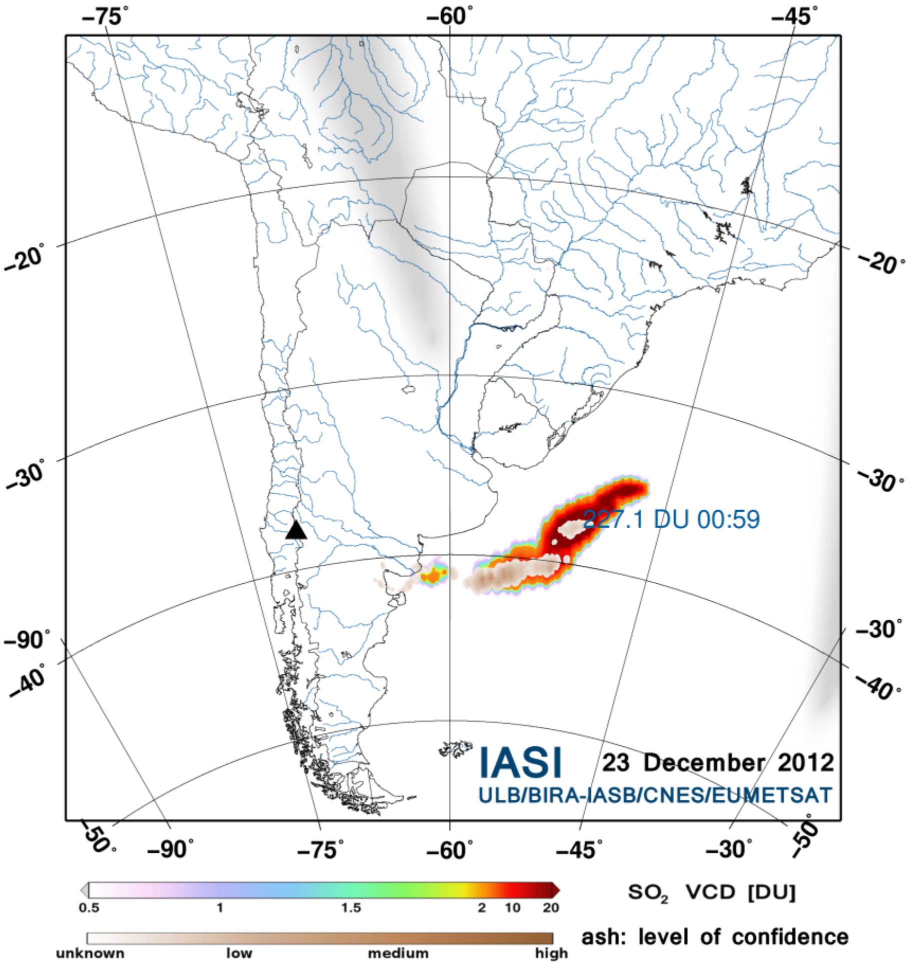

Fig. 24. SO_2 and ash detected by IASI (Copahue eruption, 23 December 2012).

NHESSD
1, 5935–6000, 2013

An online service for near real-time satellite monitoring of volcanic plumes

H. Brenot et al.

Title Page
Abstract
Introduction
Conclusions
References
Tables
Figures
◀◀
▶▶
◀
▶
Back
Close
Full Screen / Esc
Printer-friendly Version
Interactive Discussion